Chapter 1

Introduction

1.1 Idealization and Environments

Sometime between 1592 and 1610, when he taught and experimented in Padua, Galileo Galilei brought about a revolution in our understanding of nature. It was the transition from what may be described as *common sense* to an abstract, empirical interpretation of the world through mathematics, which we call *physics*.

To a casual observer various bodies fall according to their weight, an interpretation which is fully within the Aristotelian view of the world and was common in the 16th century. On the same observation, an empirical scientist - like Galilei - would point out that in vacuum all bodies fall with the same acceleration, an experimentally proven fact. This might appear like a circumvention of the problem, since in daily life bodies almost never fall in vacuum. However, this tricky approach to the problem turned out to yield a better description of the phenomenon than Aristotle's view.

The success of Galilei's concept results from the fact that it isolates the dominant process, the fall, from the multitude of minor perturbations which are caused by collisions with air molecules and dust particles. This enables a mathematical treatment of the problem which can be tested through experiments. Since Galilei's days the skill to make, for given circumstances, idealized approximations to a physical process has become the daily bread of physicists and was essential to the quantitative development of physics.

While idealizations form a sound base, an advanced description of nature needs to take into account the multitude of less important, often diverse phenomena surrounding the process of interest. Such effects cannot be treated individually. One can only imagine the impossible task of solving the equation of motion for each air molecule which collides with a falling stone. The multitude of residual degrees of freedom of a phenomenon can be combined as an *environment*, thus allowing their inclusion in the description. The environment may be modelled with macroscopic properties such as temperature, pressure, magnetic field strength, or viscous drag in the case of a falling object.

The understanding of a process is generally improved by evaluating its interactions with the surrounding environment. In many cases, like the slow fall of a feather in air, this evaluation is absolutely essential to obtain a correct description. Furthermore, only the inclusion of possible environmental degrees of freedom into the scientific model yields a holistic description of nature.

1.2 The Barrier Problem

The problem of overcoming a potential barrier is of importance in many different fields of the natural sciences. While sometimes it is an isolated phenomenon, in general, it occurs within many-particle systems and the motion across the barrier is coupled to an environment of additional degrees of freedom. Some important examples are listed in Table 1.1. The theory of the barrier problem has received

Phenomena involving potential barriers

			Environment	Impact
inversion of NH_3	Hund[3] 1927	tunnelling between two wells	atomic motion	no
α-decay	Gamow[6] 1928	tunnelling through the Coulomb barrier	internal nucleons	no
chemical reactions	Kramers[2] 1938	surmounting the activation barrier	10^{23} molecules	yes
SQUIDS	Josephson[8] 1962	tunnelling between two states of magnetic flux	electrons in junction	yes
impurities in solids	several[8] 1969	tunnelling between sites	coupling to phonons	yes

Table 1.1: *A selection of phenomena which are caused by the tunnelling or surmounting of potential barriers. The second column lists the names of researchers who are associated with the phenomenon and the year of discovery. The presence of environments of additional degrees of freedom and if they have an impact on the process are indicated in the last two columns.*

contributions from fields as diverse as atomic and nuclear physics, chemical kinetics, diffusion in solids, electric transport theory and macroscopic quantum theory. It is of interest in both classical and quantum physics[1].

1.2.1 Surmounting and Tunnelling

The physical forces acting on a particle are either *conservative* or *dissipative*. Conservative forces do not depend on time or velocity and can be expressed as the

[1]P. Hänggi, P. Talkner, M. Borkovec, Rev. Mod. Phys. **62** (1990) 251.

negative gradient of an energy potential. Since the kinetic energy is always positive or zero, energy conservation requires that the total energy of the particle, which is the sum of potential and kinetic energy, is never smaller than the potential energy. In classical physics, regions where this would be the case are forbidden. Thus classically for a particle with a certain total energy a local maximum of the energy potential which exceeds the particle's total energy constitutes a barrier which separates regions accessible to that particle.

An important example of this concept is our understanding of chemical reactions, where the potential barrier is referred to as the *activation barrier*. A reaction between two molecules takes place after the activation barrier has been surmounted. The rapidity of the chemical reaction between two substances is therefore determined by the barrier height and the temperature of the solution representing the kinetic energy of the molecules[2].

Classically a particle can only overcome a potential barrier when its total energy exceeds the barrier height. As a consequence of quantum mechanics, however, energy conservation can momentarily be violated, so that with a finite, usually small, probability the particle may tunnel through the potential barrier. This *tunnelling effect* was first recognized in the 1920's in various fields of physics. In 1927 it was demonstrated[3] that quantum mechanical tunnelling is responsible for the structural rearrangements in pyramidal molecules such as NH_3. Tunnelling became well known shortly afterwards, when the ionization of atoms in intense electric fields[4] and the electric field emission of electrons from cold metals could be described using the tunnelling mechanism[5]. In the same year the α-decay of nuclei was explained as a tunnelling effect[6,7]. Since then, quantum mechanical tunnelling has been successfully invoked to describe phenomena in a multitude of fields[8,9] in biology, chemistry and physics. Tunnelling is at the base of applications like the scanning tunnelling microscope, Zener-diodes, Josephson-junctions and superconducting quantum interference devices (SQUIDS). The fast transfer of electrons and protons in biological

[2] H.A. Kramers, Physica, The Hague, 7 (1940) 184.

[3] F. Hund, Z. Phys. **43** (1927) 805.

[4] J.R. Oppenheimer, Phys. Rev. **31** (1928) 80.

[5] R.H. Fowler, L. Nordheim, Proc. R. Soc., London, A **119** (1928) 173.

[6] G. Gamow, Z. Phys. **51** (1928) 204.

[7] R.W. Gurney, E.U. Condon, Nature, London, **122** (1928) 439.

[8] *Tunneling*, ed. J. Jortner, B. Pullman, Reidel, Boston (1986).

[9] *Tunneling in biological systems*, ed. B. Chance *et al.*, Academic Press, N.Y. (1979).

macro-molecules, optimised by evolution, proceeds entirely by tunnelling, making it one of the most fundamental processes in nature.

In physics, the barrier problem has never ceased to be of interest. Presently research concentrates on the interplay of dynamical fields with tunnelling, which has been dubbed driven tunnelling[10], the onset of chaos at the transition between the quantum mechanical and the classical description of the barrier problem[11-14], and the coupling of the barrier problem to environmental degrees of freedom[15].

1.2.2 Coupling to Environments

A particle, or a particular degree of freedom of a system may overcome a potential barrier either classically or quantum mechanically. In either case, if it belongs to a many-particle system, its motion can be strongly effected by the environment formed by the other particles. This coupling to other degrees of freedom of a many-particle system can both aid and hinder the motion across the barrier.

Figure 1.1 illustrates this *generalized barrier problem.* A particle of mass m which is coupled to an environmental many-particle system moves towards a potential barrier. The particle has the position coordinate r, carries the momentum p and confronts a barrier of the potential $V(r)$. The classical Hamiltonian of the system is then given by

$$H = \frac{p^2}{2m} + V(r) + \sum_{i=0}^{n} h_i(\alpha_i, \Pi_i) + \sum_{i=0}^{n} v_i^{coup}(r, \alpha_i) \qquad (1.1)$$

The environmental degrees of freedom, which may be infinite ($n \rightarrow \infty$), are represented by the Hamiltonians h_i. They depend on the generalized coordinates and momenta (α_i, Π_i). The coupling between the environment and the particle is expressed by the coupling potentials $v_i^{coup}(r, \alpha_i)$. For simplicity the Hamiltonian is given for the one-dimensional barrier problem. The extension of the problem to higher dimensions imposes no general restriction.

The expansion in the Hamiltonian 1.1 has three limits, which are illustrated in Figure 1.2. The first case is the *trivial limit.* It occurs when the coupling is weak.

---

[10] F. Großmann *et al.*, Phys. Rev. Lett. **67** (1991) 516.

[11] R. Utermann *et al.*, Phys. Rev. E **49** (1994) 273.

[12] M. Latka *et al.*, Phys. Rev. A **50** (1994) 1071.

[13] C.H. Dasso *et al.*, Nucl. Phys. A **549** (1992) 265.

[14] C.H. Dasso *et al.*, Nucl. Phys. A **587** (1995) 339.

[15] *Quantum Tunnelling ...* , ed. Y. Kagan, North-Holland, Amsterdam (1992).

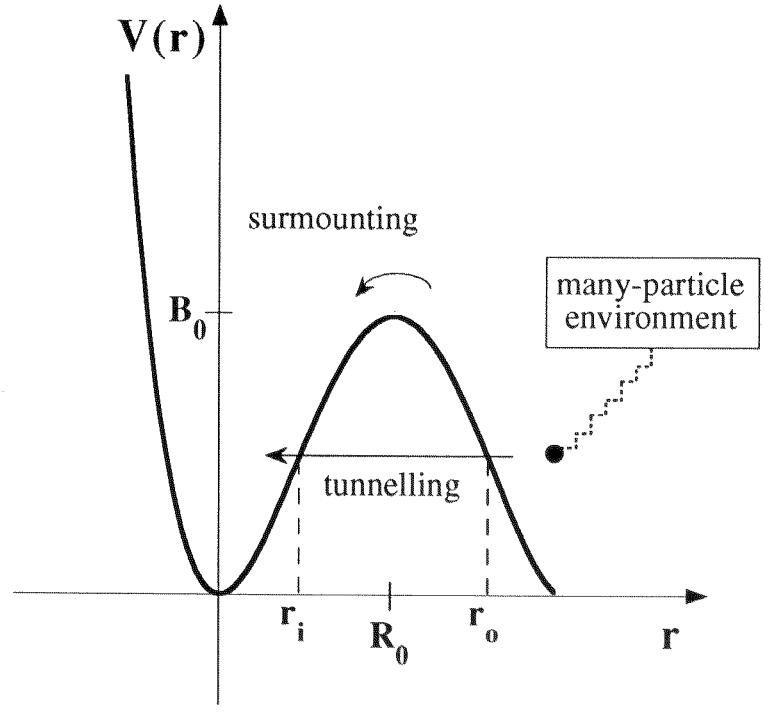

Figure 1.1: *In the generalized barrier problem the motion of a particle over or through a potential barrier of height B_0 at the position R_0 is coupled to a many-particle environment. The inner and outer turning points of the barrier are indicated by r_i and r_o, respectively.*

Then the environment may be neglected entirely. The second case is valid when the number of environmental degrees of freedom is large, their coupling similar and the individual coupling strength is weak. Using statistical theory, the microscopic Hamiltonian can then be transformed to yield a *macroscopic description*. A third case occurs, when the number of environmental degrees of freedom is limited or some of them are dominant with respect to the remainder. In this case, the infinite expansion in the Hamiltonian 1.1 may be *truncated* to include only the strong couplings.

1.2.3 The Uncoupled Barrier Problem

For a classical system in the trivial case of no coupling the transmission probability over the barrier switches from 0 to 1 when the particle's energy E equals the barrier height B_0. For energies below B_0 the transmission probability is 0, for energies above B_0 it is 1. In quantum mechanics this step-function is smoothed because of tunnelling. The smoothed transmission function can be calculated using the

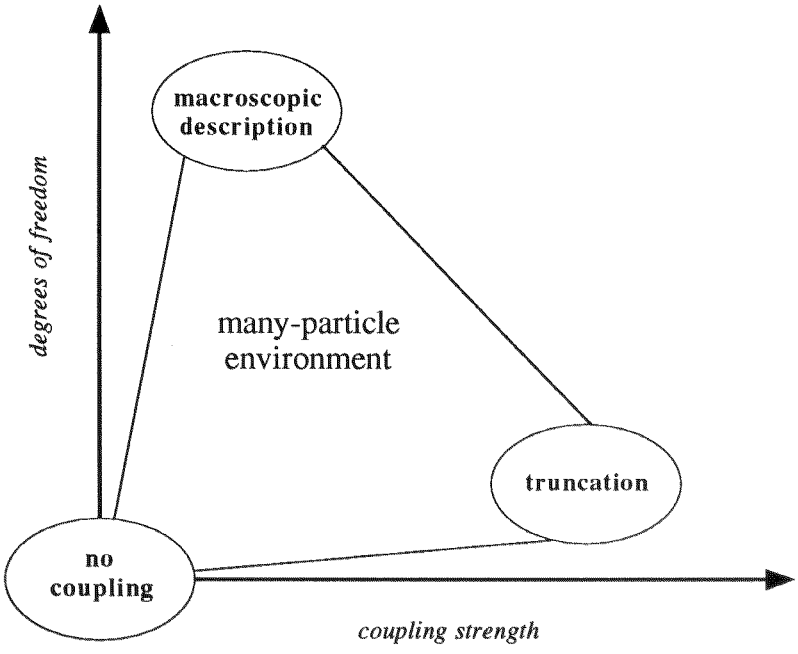

Figure 1.2: *The three limits of environmental coupling.*

Wentzel-Kramers-Brillouin method[16,17]. With the integral

$$K(E) = \pm \int_{r_i}^{r_o} \sqrt{\frac{2m}{\hbar^2}|V(r) - E|}dr \tag{1.2}$$

where $\hbar$ is Planck's constant divided by 2π and r_i and r_o refer to the inner and outer turning points of the barrier, the barrier transmission function is given by

$$T(E) = (1 + \exp[2K(E)])^{-1} \tag{1.3}$$

The minus and plus signs in front of the integral in Equation 1.2 correspond to energies E above or below B_0, respectively.

A barrier shape which is of interest because of its mathematical simplicity is that of an inverted parabola. It may be expressed as

$$V(r) = B_0 - \frac{m\omega_0^2}{2}(r - R_0)^2 \tag{1.4}$$

[16]E.C. Kemble, Phys. Rev. **48** (1936) 549.

[17]N. Froman, P.O. Froman, *JWKB Approximation*, North-Holland, Amsterdam (1965).

where R_0 is the barrier position and $\omega_0 = \sqrt{-V''/m}$ is the eigen-frequency of the harmonic oscillator with the potential $V(r)$. The transmission function for this special case is given by[18]

$$\mathcal{T}(E) = \left(1 + \exp\left[\frac{2\pi}{\hbar\omega_0}(B_0 - E)\right]\right)^{-1} \tag{1.5}$$

When the energy equals the barrier height B_0, the transmission is only 0.5, whereas at energies below B_0 it can be considerably larger than zero. $\mathcal{T}(E)$ increases from 0.1 to 0.9 as the energy increases from $B_0 - 1.1\hbar\omega_0$ to $B_0 + 1.1\hbar\omega_0$.

While the isolated and uncoupled barrier problem is almost always an idealization, the radioactive α-decay[19–21] and the field ionization of atoms[22] are important examples, where this idealization can be justified.

1.2.4 Macroscopic Description

In the case where many, maybe an infinite number of environmental degrees of freedom couple to the motion across the barrier, the exact microscopic Hamiltonian is generally not known. Thus the modelling of the many-particle environment has to rely on appropriate assumptions about the nature of the couplings. Often the schematic model of a heat-bath is employed.

The most general realization of a heat-bath is the independent oscillator model, in which the particle overcoming the barrier is coupled to an infinite number of heat-bath particles, each attached by a spring. The corresponding Hamiltonians are

$$h_i(\alpha_i, \Pi_i) = \frac{\Pi_i^2}{2m_i} + \frac{1}{2}m_i\omega_i^2\alpha_i^2 \tag{1.6}$$

where the m_i and ω_i are the masses of the heat-bath particles and the eigen-frequencies of the springs, respectively, and $i = 0, 1, ...\infty$.

The coupling potentials are given by

$$v_i^{coup}(r, \alpha_i) = r\lambda_i\alpha_i + r^2\frac{\lambda_i^2}{2m_i\omega_i^2} \tag{1.7}$$

where the λ_i are coupling constants.

[18] D.L. Hill, J.A. Wheeler, Phys. Rev. **89** (1953) 1102.

[19] S. Biwas, Phys. Rev. **75** (1949) 530.

[20] D.F. Jackson, M. Rhoades-Brown, Ann. Phys. **105** (1977) 151.

[21] E. Roeckl, Nucl. Phys. A **400** (1983) 131c.

[22] J.R. Oppenheimer, Proc. Nat. Acad. Sci., U.S.A. **14** (1928) 363.

With the expressions 1.6 and 1.7 the Hamiltonian 1.1 becomes cumbersome. This ansatz, however, leads to the macroscopic models of *transport theory* which are based on differential equations such as the Fokker-Planck and Langevin equations[23,24]. It has been shown[25] that this relationship between the independent oscillator model and the macroscopic differential equations is also valid in the quantum mechanical case, if the classical quantities are replaced by operators in the conventional way.

With additional assumptions the Langevin equation may be expressed as

$$\dot{p} = -\frac{dV}{dr} - \gamma(r)\dot{r} + \xi(t)\sqrt{\gamma(r)kT} \tag{1.8}$$

The assumptions include that the spectrum of oscillation frequencies is quadratic, that the frequency integration is to infinity and that the heat-bath is in thermal equilibrium. In Equation 1.8 the second term represents a dissipative *friction force* which is proportional to the particle velocity $\dot{r}$ with a friction form factor $\gamma(r)$. The third term is a *fluctuating force*, whereby $\xi(t)$ is a stochastic function of time, k the Boltzmann constant and T is the temperature of the heat-bath. Thus in the macroscopic limit the couplings can be related to fluctuations and energy dissipation in the many-particle environment, which can be quantified using the macroscopic environmental properties of temperature and friction.

Based on the concepts which have just been described, macroscopic transport theory has been a successful approach to barrier problems with large environments of additional degrees of freedom[26]. When the heat-bath is of a quantum mechanical nature the classical approach can be extended[27,28]. This case is of particular interest in the discussion about quantum mechanics and realism at the macroscopic level[29] which is based on SQUIDS. In such devices, transitions between two discrete values of the magnetic flux are interpreted as collective or macroscopic tunnelling between two potential wells. In the absence of dissipation these systems would be essentially equivalent to the hypothetical cat of Erwin Schrödinger's famous gedanken experiment and they would allow the observation of coherent superpositions of two

[23]D.H.E. Gross, Lec. Not. Phys. **117** (1980) 81.

[24]P. Fröbrich, Springer Proc. Phys. **58**, Springer, Berlin (1991) 93.

[25]G.W. Ford, J.T. Lewis, R.F. O'Connell, Phys. Rev. A **37** (1988) 4419.

[26]P. Hänggi, P. Talkner, M. Borkovec, Rev. Mod. Phys. **62** (1990) 251.

[27]R.P. Feynman, F.L. Vernon, Ann. Phys., N.Y., **24** (1963) 118.

[28]R.P. Feynman, A.R. Hibbs, *Quantum mechanics and ...* , McGraw Hill, N.Y. (1965).

[29]A.J. Leggett, Prog. Theo. Phys. Suppl. **69** (1980) 80; Contemp. Phys. **25** (1984) 583.

macroscopic quantum states. This would be an experimental test of the quantum mechanical measurement problem. However, despite their operation at temperatures near absolute zero, SQUIDS show residual dissipation because of the thermal motion of electrons[30]. Progress in these experiments will depend critically on the understanding of the coupling between the tunnelling and the environment of thermal electrons.

1.2.5 Truncation

Sometimes it may be physically sensible to limit the environmental degrees of freedom i to a discrete, possibly small number n with $i = 0, 1, .., n$. Then the classical Hamiltonian 1.1 leads to a coupled system of differential equations which describe the particle's motion over the barrier.

In the quantum mechanical picture, a discrete number of environmental degrees of freedom may be represented as a complete and orthonormal system of eigenfunctions $\chi_i(\alpha_i)$ with

$$\int \chi_j^*(\alpha_j)\chi_i(\alpha_i)d\alpha_i = \delta_{ji} \tag{1.9}$$

where δ_{ji} is the Kronecker symbol and the asterisk indicates complex conjugation. For simplicity it is assumed that the environmental degrees of freedom do not depend on their generalized momenta Π_i. This enables the wave function Ψ of the generalized barrier problem to be expanded in terms of the eigen-functions $\chi_i(\alpha_i)$

$$\Psi(r, \alpha_0, .., \alpha_i, .., \alpha_n) = \sum_{i=0}^{n} \phi_i(r)\chi_i(\alpha_i) \tag{1.10}$$

In this expansion, the coefficients ϕ_i depend only on the coordinate r of the particle. Inserting the wave function Ψ and the quantum mechanical equivalent of the Hamiltonian 1.1 into the Schrödinger equation

$$[H - E]\,\Psi = 0 \tag{1.11}$$

yields the equation

$$\sum_{i=0}^{n} \left[-\frac{\hbar^2}{2m}\frac{d^2}{dr^2} + V(r) + v_i^{coup}(r, \alpha_i) - E + \epsilon_i \right] \phi_i(r)\chi_i(\alpha_i) = 0 \tag{1.12}$$

where the ϵ_i are the energy eigen-values of the environmental degrees of freedom with

$$[h_i - \epsilon_i]\,\chi_i(\alpha_i) = 0 \tag{1.13}$$

[30] A.O. Caldeira, A.J. Leggett, Phys. Rev. Lett. **46** (1981) 211; Ann. Phys. **149** (1983) 374.

If Equation 1.12 is multiplied from the left with $\chi_j^*(\alpha_j)$ and integrated over α_i for all i, the orthogonality property (1.9) of the eigen-functions can be applied. One obtains the following system of coupled equations with $j = 0, 1, .., n$

$$\left[-\frac{\hbar^2}{2m}\frac{d^2}{dr^2} + V(r) - E\right]\phi_j(r) = -\sum_{i=0}^{n} M_{ji}(r)\phi_i(r) \tag{1.14}$$

The $M_{ji}(r)$ are the elements of the *coupling matrix*, with

$$M_{ji}(r) = \int \chi_j^*(\alpha_j) v_i^{coup}(r, \alpha_i)\chi_i(\alpha_i)d\alpha_i + \epsilon_i\delta_{ji} \tag{1.15}$$

The integration is over the environmental degrees of freedom α_i, consequently the matrix elements remain a function of the position coordinate r. Assuming time reversal invariance it follows that $M_{ji} \equiv M_{ij}$. Furthermore it is $M_{ii} \equiv \epsilon_i$. The coupled equations (1.14) can be solved numerically when the matrix elements $M_{ji}(r)$ are known. Then the wave function Ψ and the barrier transmission function $\mathcal{T}(E)$ can be calculated.

Truncation of the Hamiltonian as a limit of environmental coupling has its natural application in solid state physics, chemistry and biophysics. It is applied to processes like the tunnelling of defects in crystals[31], diffusion of interstitials in metals[32], the tunnelling of electrons in insulators[33], chemical reactions[34] and the rearrangements of biomolecules[35]. In all these cases, the tunnelling couples to elastic and inelastic modes, e.g. phonons, of the surrounding atoms or molecules. While in general macroscopic systems consist of the order of 10^{23} atoms, only the closest neighbours have a decisive influence on the tunnelling motion. This limits the environmental degrees of freedom considerably and justifies the truncation of the Hamiltonian.

1.3 Environmental Coupling in Nuclei

Environmental coupling can have a considerable impact on the ubiquitous and fundamental barrier crossing problem. A study of this impact as a function of the nature and the strength of the coupling should therefore yield a better and more

[31] V. Narayanamurti, R.O. Pohl, Rev. Mod. Phys. **42** (1970) 201.

[32] C.P. Flynn, A.M. Stoneham, Phys. Rev. B **1** (1970) 3966.

[33] T. Holstein, Ann. Phys., N.Y. **8** (1959) 343.

[34] T.F. George, W. H. Miller, J. Chem. Phys. **56** (1972) 5722.

[35] J.J. Hopfield, Proc. Nat. Acad. Sci., U.S.A. **71** (1974) 3640.

comprehensive understanding of this problem. Such a study requires a physical system which accommodates the three limits which have been presented in the preceding sections. Furthermore, the system should enable the coupling strength to be varied in a controlled manner.

While various kinds of environments with different coupling strengths are realized among the many manifestations of the barrier problem, the environmental properties are usually fixed and cannot be altered. There exists, however, a unique system, which enables a large amount of environmental tuning. This system is the atomic nucleus.

1.3.1 The Nuclear Many-Particle System

Atomic nuclei can consist of only a few or several hundred nucleons. The nucleons are independent particles and interact with each other through nuclear and electromagnetic forces. The forces between two nucleons are well known from scattering experiments and one may feel encouraged to deduce nuclear properties directly from these two-body interactions. Calculating several hundred wave functions is however cumbersome and the individual degrees of freedom of the protons and neutrons inside the nucleus may instead rather be considered to form an environment for the dominant nuclear processes such as scattering, fusion, fission or decay.

The nuclear environment is *internal* in character, in contrast to our usual perception of environments as *external* entities. The nucleons are confined by the attractive nuclear force into a small volume with a well defined boundary and which is isolated in space. The distance from the nuclear surface to the closest electron is typically more than a thousand times the nuclear diameter. The number of internal degrees of freedom increases as $3A$, where A is the nuclear mass number. When the excitation energy of the nucleus is large, the nucleus behaves almost like a classical many-particle system. This makes possible the gradual change of the size of the environment by going from light to heavy nuclei. Considering that the nucleons are fermions with spin $\pm\frac{1}{2}$, the total number of internal degrees of freedom for a heavy nucleus like ^{208}Pb is of the order of 10^3.

At low excitation energies the independent-particle character of the system is modified by the properties of the nuclear mean-field which arises from the superposition of the inter-nucleon forces[36]. The mean-field imposes a structure on the nucleus, which confines its inner core into stable shells of neutrons or protons. This

[36]A. Bohr, B. Mottelson, *Nuclear Structure*, Vol. I, Benjamin, Reading (1969).

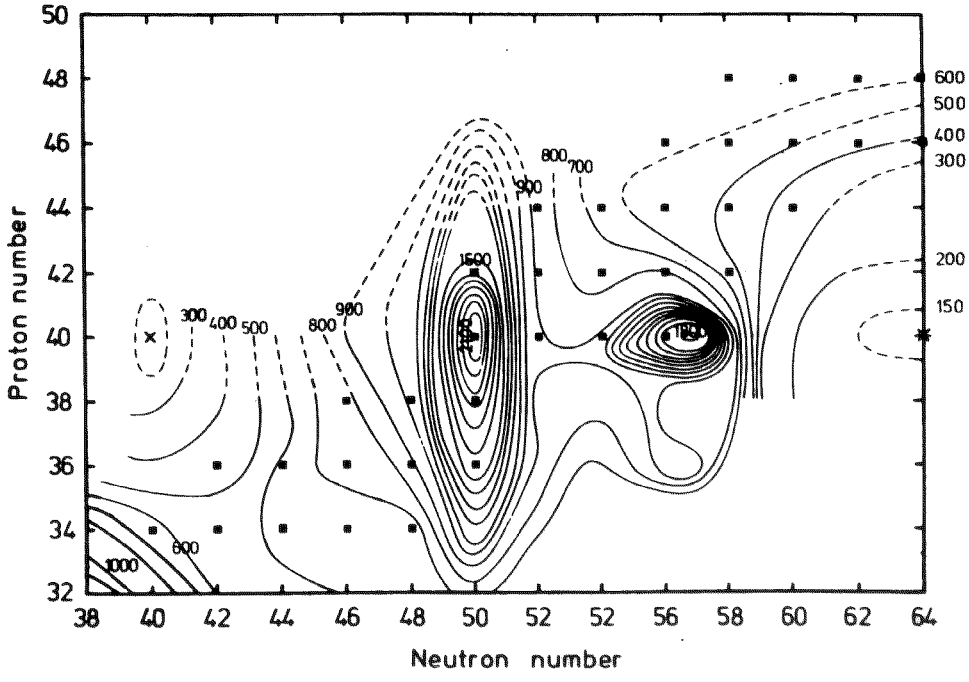

Figure 1.3: *Contour map of the experimental excitation energies of the lowest 2^+ state for even-even nuclei in the region $70 < A < 110$ as a function of proton and neutron number.*

stabilization leaves only the valence nucleons outside the closed shells to be excited. As a consequence, there exist closed shell nuclei like ^{40}Ca in which internal degrees of freedom are difficult to excite. Successive addition of nucleons or nucleon holes to these inert configurations softens the nucleus and leads quickly to a large number of low energy states.

Particularly strong degrees of freedom arise when the valence nucleons combine their motion collectively as rotations or vibrations[37]. These collective states dominate the excitation spectrum at low energies and can successfully be described in terms of a quantum mechanical vibrator or rotor. The spectrum of the collective states and their coupling strength can change dramatically. This is illustrated[38] for even-even nuclei with $70 < A < 110$ in Figure 1.3, which shows a contour plot of the experimental excitation energies of the lowest energy 2^+ state. The energy maxima occur for $^{90}_{40}Zr_{50}$ and $^{96}_{40}Zr_{56}$ corresponding to the $N = 50$ closed shell and the $N = 56$ closed $d_{5/2}$ subshell, respectively. In both nuclei the 2^+ state is only

[37]A. Bohr, B. Mottelson, *Nuclear Structure*, Vol. II, Benjamin, Reading (1975).

[38]I. Ragnarsson, S.G. Nilsson, R.K. Sheline, Phys. Rep. **45** (1978) 1.

moderately collective. The successive addition or subtraction of nucleons, however, strongly reduces the excitation energy of the lowest 2^+ state, which is an indication of an increase in collectivity.

By selecting the size, nuclear structure and excitation energy of the nuclear many-particle system appropriately, a broad range of environmental conditions can be investigated.

1.3.2 The Coulomb Barrier

Besides diverse environments, a study of their coupling to the barrier problem requires a well defined potential barrier. Such a barrier arises in the *nuclear binary problem*, when two nuclei combine in nuclear fusion, as the *Coulomb barrier*, or when a single nucleus fissions into two fragments, as the fission barrier. The positive charges of the protons induce a long range and repulsive electrostatic Coulomb force. At inter-nuclear separations of the order of the nuclear diameter, this force is superimposed with the short-range, attractive nuclear force, which is the residual of the unsaturated hadronic forces stabilizing the nucleons.

As in the Kepler problem, in the nuclear binary problem the two partners are of comparable mass, so that the system is more easily described in terms of their relative motion in the centre-of-mass system. Assuming the standard laboratory situation of a fixed target which is bombarded with a beam of projectile nuclei, the relation between the kinetic energy E_{lab} as measured in the laboratory system and the kinetic energy E_{cm} in the centre-of-mass system is given by

$$E_{cm} = \frac{A_t}{A_p + A_t} E_{lab} \tag{1.16}$$

where A_p and A_t represent the mass numbers of the projectile and target nuclei, respectively. Electron masses and differences in binding energy per nucleon may be ignored to good approximation.

The motion of the centre-of-mass is fully determined by the kinematics of the reaction and can be calculated from the bombarding energy and the nuclear masses. The possibly complicated dynamics of the reaction is entirely reflected in the relative motion of the nuclei in the centre-of-mass system. The binary problem therefore reduces to a one-body problem for the relative coordinate r and the reduced mass

$$\mu = \frac{A_p A_t}{A_p + A_t} m_N \tag{1.17}$$

where m_N is the nucleon mass. At centre-of-mass energies of the order of the Coulomb barrier height the relative velocities of the nuclei are typically less than 10% of the velocity of light, so that the relative motion can be treated non-relativistically.

Quantum-mechanically the nuclear binary system may be represented by the wave-function $\Psi(r)$. Using the centre-of-mass parametrization, the combined effect of the Coulomb and the nuclear force between the two nuclei can be expressed as the interaction potential

$$V(r) = V_C(r) + V_n(r) \tag{1.18}$$

where V_C is the Coulomb and V_n the nuclear potential. The motion of the binary system is then described by the Schrödinger equation

$$\left[-\frac{\hbar^2}{2\mu}\frac{d^2}{dr^2} + V(r) - E\right]\Psi(r) = 0 \tag{1.19}$$

At large distances r, the Coulomb potential V_C has the form of the electrostatic potential for two point-charges. At close approach, when the charge distributions overlap, the point-charge idealization has to be modified. This is often realized by replacing one of the point-charges with a homogeneously charged sphere of radius R_C, so that

$$V_C(r) = Z_p Z_t e^2 \begin{cases} 1/r & \text{for } r > R_C \\ (\frac{3}{2} - \frac{r^2}{2R_C^2})/R_C & \text{for } r \leq R_C \end{cases} \tag{1.20}$$

where Z_p and Z_t represent the nuclear charge numbers of the projectile and target nuclei, respectively.

Since during the collision there occur a large number of interactions between the projectile and target nucleons, it has not been possible to determine the nuclear potential V_n from the known two-body forces between nucleons. It is therefore common to make a simple parametrization, approximating the nuclear potential with a function which resembles the nuclear mass distribution. This leads to the Woods-Saxon potential

$$V_n(r) = \frac{-V_0}{1 + \exp(\frac{r - R_n}{a_0})} \tag{1.21}$$

where V_0 refers to the potential depth and a_0 is the diffuseness of the potential. The radius R_n of the nuclear potential is given by

$$R_n = r_0(A_p^{1/3} + A_t^{1/3}) \tag{1.22}$$

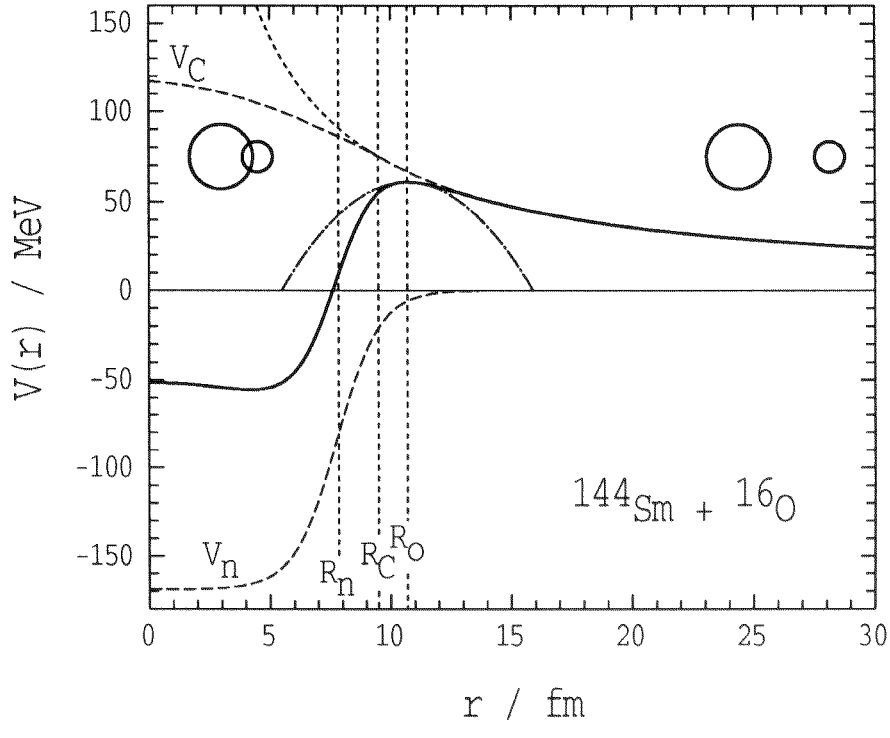

Figure 1.4: *The interaction potential $V(r)$ (solid) for $^{144}Sm + {}^{16}O$ in a head-on collision. The potential is the sum of the Coulomb potential V_C and the nuclear potential V_n (long-dashed curves). At its vertex, the potential barrier may be approximated with an inverted parabola (dot-dashed). The point-charge approximation of the Coulomb potential is shown as short-dashed curve. The radial distances R_n, R_C and R_0 are defined in the text. The approximate relative dimensions and separations of the nuclei outside and inside the barrier are depicted by the circles.*

where r_0 is the radius parameter. The potential parameters V_0, a_0 and r_0 are not unique. They are usually adjusted to fit experimental data.

Figure 1.4 shows the interaction potential $V(r)$ and its components V_C and V_n for the system ^{144}Sm + ^{16}O. The competition between the electrostatic and the nuclear forces gives rise to a potential barrier at the distance R_0. At its vertex the shape of the barrier may be approximated by an inverted parabola[39]. Since this is generally a good approximation at energies close to the barrier height, the exact potential is often replaced by this function.

When two nuclei overcome the Coulomb barrier and reach the potential pocket they can form a composite system and fuse. In the opposite direction, a single nucleus can overcome the analogous but different fission barrier to scission into two

[39]T.D. Thomas, Phys. Rev. **116** (1959) 703.

unbound fragments in the process of fission[40]. The motion over the barrier can couple to the internal degrees of freedom of the nuclei, which include excitations and mass transfer. The effects of this coupling are observed both in fusion and fission. However, by selecting different projectile-target combinations different environmental conditions can be well chosen for fusion, whereas this is not so easy for fission. Thus fusion is the preferred process to investigate the environmental coupling of the nuclear barrier problem.

1.4 Nuclear Fusion

The fusion of two nuclei[41–46] may be defined as the confinement of the binary system inside the potential barrier and the formation of a *compound nucleus* with charge $Z_c = Z_p + Z_t$ and mass $A_c = A_p + A_t$. The term compound nucleus is used to indicate Niels Bohr's hypothesis[47] that the newly formed nucleus quickly loses memory of its formation. This implies equilibration of all internal degrees of freedom.

In general the compound nucleus is initially in a highly excited state which decays via particle emission[48] or fission[49] and subsequent γ-ray emission, as illustrated in Figure 1.5. The high density of states at these energies enables a description of this decay within the statistical model[50]. In lighter nuclei, with $Z_c \lesssim 70$, the probability of fission is typically so small that essentially all decays proceed via particle emission. Within the terminology of the statistical model, particle emission is often referred to as particle evaporation. The evaporated particles are dominantly neutrons, but also protons and α-particles. This decay mode results in nuclei close in mass to the compound nucleus, dubbed *evaporation residues*. In the decay of heavier compound nuclei with $Z_c \gtrsim 70$, fission competes successfully with particle evapo-

[40] D. Hilscher, H. Rossner, Ann. Phys. **17** (1992) 471.

[41] *Fusion Reactions* ..., Lec. Not. Phys. **219**, ed. S.G. Steadman, Springer (1985) 351.

[42] S.G. Steadman, M.J. Rhoades-Brown, Ann. Rev. Nucl. Part. Sci. **36** (1986) 649.

[43] W. Reisdorf, Inst. Phys. Conf. Ser. No. **86**, Int. Nucl. Phys. Conf. (1986) 205.

[44] M. Beckerman, Rep. Prog. Phys. **51** (1988) 1047.

[45] W. Reisdorf, J. Phys. G: Nucl. Part. Phys. **20** (1994) 1297.

[46] *Heavy Ion Fusion*, Conf. Proc., ed. A.M. Stefanini, World Scientific, Singapore (1994).

[47] N. Bohr, Nature **137** (1936) 344.

[48] V. Weisskopf, Phys. Rev. **52** (1937) 295.

[49] N. Bohr, J.A. Wheeler, Phys. Rev. **56** (1939) 426.

[50] V.L. Weisskopf, J.M. Blatt, *Theoretical Physics*, Wiley, N.Y. (1952).

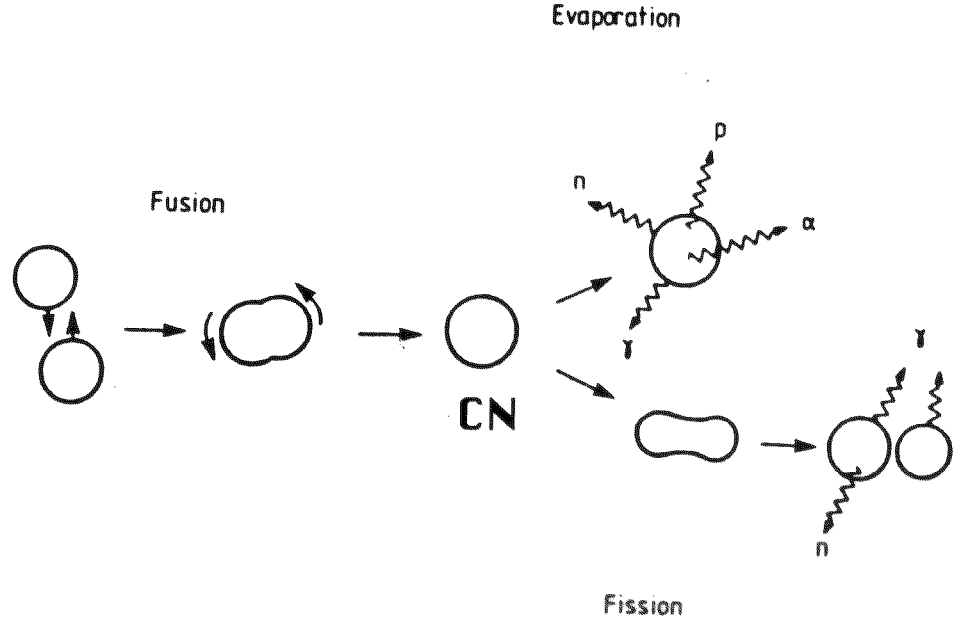

Figure 1.5: *Formation and decay of the compound nucleus (CN).*

ration and dominates for large Z_c even at energies below the barrier height[51-53].

For heavy compound nuclei, where fission is important, it is not necessarily straight-forward to establish experimentally that an equilibrated compound nucleus has been formed. The fission barrier may be located inside the fusion barrier, so that a *quasi-fission* process of the unequilibrated composite system is observed in addition to fission after compound nucleus formation[54,55]. Furthermore, because of the large overlap, deep-inelastic reactions with a massive loss of energy and an exchange of many nucleons occur for heavy systems resulting in reaction products which may be similar to fission fragments. While deep-inelastic reaction have to be rejected both the evaporation residue cross section and the fission cross section have to be measured in order to establish the fusion cross section. It has been argued[56] that in investigations of the fusion barrier problem the fission cross section must include quasi-fission reactions, since for quasi-fission to occur the system has to

[51]J.R. Leigh *et al.*, Phys. Rev. Lett. **48** (1982) 527.

[52]D.J. Hinde *et al.*, Nucl. Phys. A **385** (1982) 109.

[53]F. Plasil *et al.*, Phys. Rev. C **29** (1984) 1145.

[54]B. Borderie *et al.*, Z. Phys. A **299** (1981) 263.

[55]B.B. Back, Phys. Rev. C **31** (1985) 2104.

[56]D.J. Hinde *et al.*, Nucl. Phys. A **592** (1995) 271.

overcome the fusion barrier.

1.4.1 Fusion Excitation Functions

By extending the theoretical description to three spatial dimensions, it has to be taken into account that the interaction potential $V_\ell(r)$ depends on the orbital angular momentum $\ell\,\hbar$ with

$$V_\ell(r) = V(r) + V_{cent}(r, \ell) \tag{1.23}$$

where $V(r)$ is given by Equation 1.18 and $V_{cent}(r, \ell)$ is the centrifugal term with

$$V_{cent}(r, \ell) = \frac{\hbar^2}{2\mu r^2}\ell(\ell+1) \tag{1.24}$$

As illustrated in Figure 1.6, the centrifugal potential increases the barrier height and shifts the barrier position to smaller radii with rising orbital angular momentum. For large ℓ it eventually fills in the attractive pocket and thus restricts fusion to the small angular momenta.

For an angular momentum dependent potential the transmission function becomes also angular momentum dependent with $\mathcal{T}(E) \equiv \mathcal{T}_\ell(E)$ and for each ℓ the fusion probability can be expressed as the differential cross section

$$\sigma_\ell^{fus}(E) = \pi\lambda^2(2\ell+1)\mathcal{T}_\ell(E) \tag{1.25}$$

where $\lambda = \hbar/p$ is the reduced de Broglie wavelength associated with the relative motion. By summing over all angular momenta, the total fusion cross section is obtained as

$$\sigma^{fus}(E) = \sum_{\ell=0}^{\infty} \sigma_\ell^{fus}(E) \tag{1.26}$$

This energy dependent function is generally referred to as the *fusion excitation function.*

1.4.2 The One-Dimensional Model

The transmission probability $\mathcal{T}_\ell(E)$ over the barrier can be calculated by numerically solving the Schrödinger equation (1.19) with the boundary conditions that for large distances the incoming wave function of the binary system is a plane-wave and the outgoing wave function is a radial-wave, thus

$$\Psi(r) \overset{r\to\infty}{\longrightarrow} N\left[\exp(ikz) + f(\theta)\frac{1}{r}\exp(ikr)\right] \tag{1.27}$$

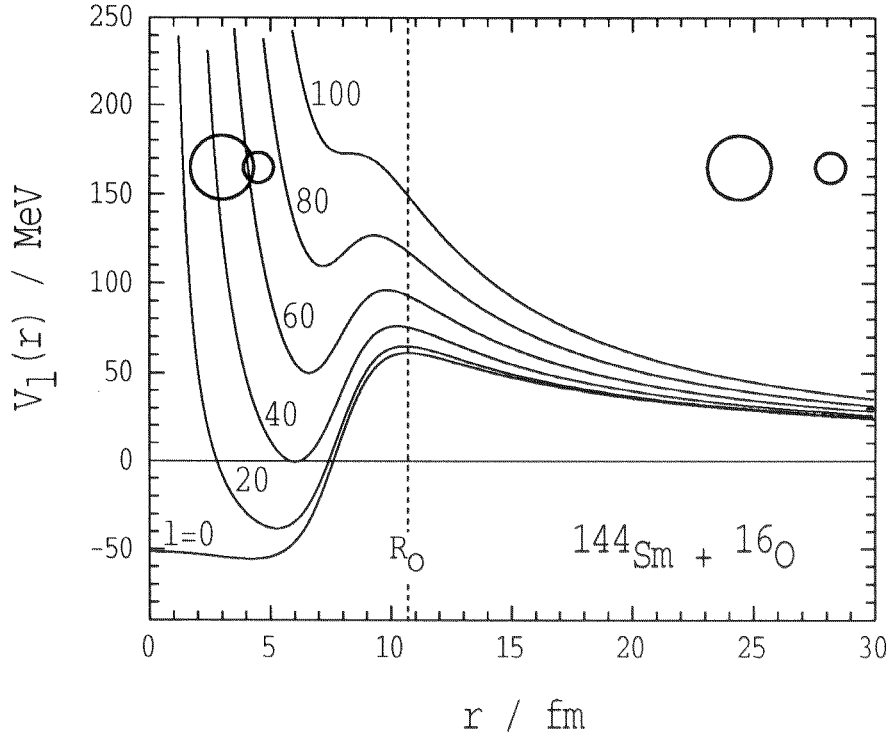

Figure 1.6: *The interaction potentials $V_\ell(r)$ for $^{144}Sm + ^{16}O$ as a function of angular momentum ℓ. R_0 indicates the position of the barrier for $\ell = 0$.*

where the factor N normalizes the wave function to unity, $k = 1/\lambda$ is the wave number, z is the coordinate in the beam direction, and $f(\theta)$ is the scattering amplitude. Absorption into the fusion channel is simulated by requiring that inside the barrier the amplitude of the wave function vanishes. The latter can be achieved by introducing an absorptive imaginary term[57] $W(r)$ in the potential, so that $V_\ell(r)$ is replaced by $U_\ell(r)$ with

$$U_\ell(r) = V_\ell(r) + W(r) \tag{1.28}$$

The imaginary part may have the Woods-Saxon form

$$W(r) = \frac{-iW_0}{1 + \exp(\frac{r - R_w}{a_w})} \tag{1.29}$$

where W_0, a_w and R_w are the potential parameters and i is the imaginary unit. In order to confine $W(r)$ to distances inside the barrier, the parameters are often chosen so that $R_w \leq R_n < R_0$ and $a_w \approx a_0$. The potential depth W_0 has to be large

[57]M.J. Rhoades-Brown, P. Braun-Munzinger, Phys. Lett. B **136** (1984) 19.

enough to ensure complete absorption. Because of this feature, which is similar to the absorption of light by a black sphere, the description has been dubbed the optical model. Alternatively, absorption can be simulated using an in-going wave boundary condition[58,59].

For a parabolic barrier shape the transmission functions $\mathcal{T}_\ell(E)$ can be calculated analytically using Equation 1.5, so that

$$\mathcal{T}_\ell(E) = \left(1 + \exp\left[\frac{2\pi}{\hbar\omega_\ell}(B_\ell - E)\right]\right)^{-1} \tag{1.30}$$

where B_ℓ is the barrier for angular momentum $\ell\,\hbar$. When the width and position of the parabola are chosen so that it fits the vertex of the barrier of the exact potential, there is good agreement between this approximation and the numerical optical-model calculation.

Applying the additional assumptions that the barrier position R_0 and the barrier curvature $\hbar\omega_0$ do not change with angular momentum, and replacing the sum in Equation 1.26 by an integral, yields the following analytical expression for the fusion excitation function[60]

$$\sigma^{fus}(E) = \frac{\hbar\omega_0 R_0^2}{2E} \ln\left(1 + \exp\left[\frac{2\pi}{\hbar\omega_0}(E - B_0)\right]\right) \tag{1.31}$$

where B_0, R_0, $\hbar\omega_0$ are the barrier height, position and curvature for $\ell = 0$, respectively. At energies $E \gg B_0$, Equation 1.31 simplifies to the classical formula for the capture of a charged particle by a nucleus[61]

$$\sigma^{fus}(E) = \pi R_0^2(1 - B_0/E) \tag{1.32}$$

Because of the approximate treatment of the angular momentum dependence, Equations 1.31 and 1.32 generally overpredict the fusion cross section at energies $E > B_0$. Expanding the logarithm in Equation 1.31 leads for $E \ll B_0$ to the approximation

$$\sigma^{fus}(E) \approx \frac{\hbar\omega_0 R_0^2}{2E} \exp\left[\frac{2\pi}{\hbar\omega_0}(E - B_0)\right] \tag{1.33}$$

In the description of nuclear fusion as presented above the potential $V_\ell(r)$ depends apart from the angular momentum $\ell\,\hbar$, which is a constant of motion, only

[58]G.H. Rawitscher, Nucl. Phys. A **85** (1966) 337.

[59]S. Landowne, S.C. Pieper, Phys. Rev. C **29** (1984) 1352.

[60]C.Y. Wong, Phys. Rev. Lett. **31** (1973) 766.

[61]V. Weisskopf, Phys. Rev. **52** (1937) 295.

on the radial distance r. Thus the description is essentially based on a single parameter and it is equivalent to the trivial limit of the generalized barrier problem discussed in Section 1.2.3. This description is therefore often referred to as the *one-dimensional model* picturing fusion as follows: During the reaction the projectile and target nuclei are inert spheres. However, trajectories which reach inside the barrier are assumed to irreversibly lead to fusion because of the onset of strong dissipation as a result of the inter-nucleon forces induced by the geometric overlap.

There have been attempts to empirically derive a set of potential parameters which yield a global fit to fusion excitation functions within the one-dimensional model. Christensen and Winther[62] derived such a potential from elastic scattering data. Bass obtained a global potential by fitting fusion cross sections above the barrier within a classical model of fusion[63,64]. In both cases the fits included data for systems with $50 \lesssim Z_pZ_t \lesssim 850$. The two global potentials deduced from these two independent analyses are surprisingly similar, despite the methodical differences in their derivations. For light systems with $25 \lesssim Z_pZ_t \lesssim 100$ fusion excitation functions calculated in the one-dimensional model using these empirical potentials are in good agreement with the experimental data. For systems with $100 \lesssim Z_pZ_t \lesssim 1500$ the model is reliable for centre-of-mass energies $E_{cm} \gtrsim 1.1B_0$ with only few exceptions.

The one-dimensional, empirical approach fails, however, for systems with $Z_pZ_t \gtrsim 100$ at energies $E_{cm} \lesssim 1.1B_0$, and for heavy systems with $Z_pZ_t \gtrsim 1500$ at all energies. Enhancements of the fusion cross sections of up to several orders of magnitude compared to the predictions of the one-dimensional model are observed at energies $E \lesssim B_0$. This effect has been named *sub-barrier fusion enhancement*. In addition, for $Z_pZ_t \gtrsim 1500$ the experimentally derived fusion barriers B_0 are much higher than predicted by the empirical potentials. This phenomenon has been dubbed *fusion hindrance*.

1.4.3 Sub-Barrier Fusion Enhancement

The sub-barrier enhancement of fusion excitation functions is demonstrated in Figure 1.7 for the systems $^{16}O + {}^{144,148,154}Sm$. The excitation functions of the three reactions have been normalized to each other by dividing the energies by the re-

[62] P.R. Christensen, A. Winther, Phys. Lett. B **65** (1976) 19.

[63] R. Bass, Phys. Rev. Lett. **39** (1977) 265.

[64] R. Bass, Lec. Not. Phys. **117**, Springer, Berlin (1980) 281.

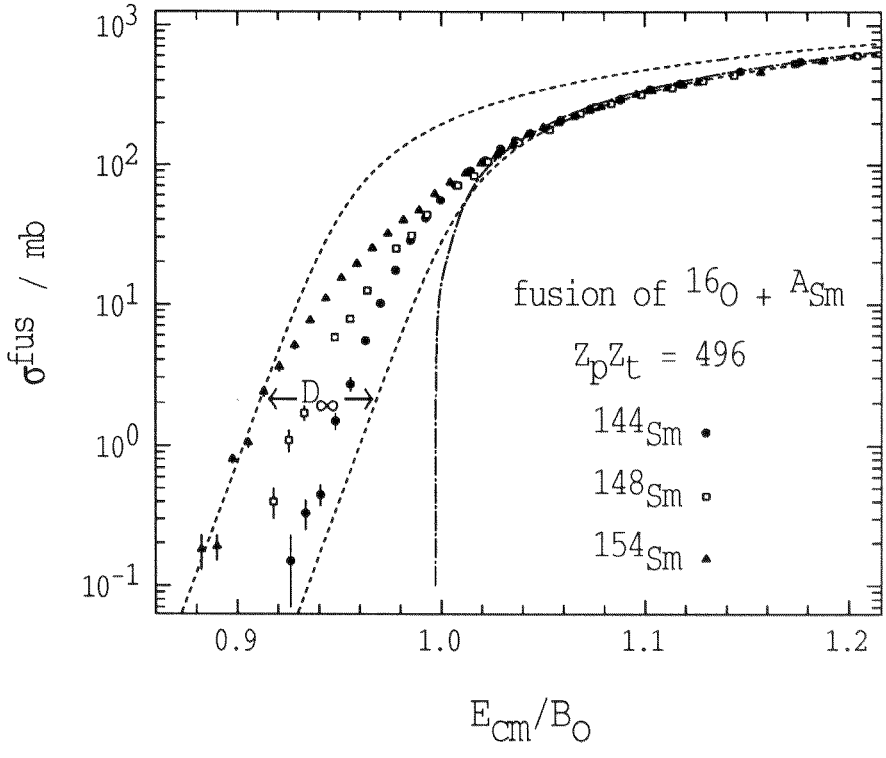

Figure 1.7: *The fusion excitation functions for ^{16}O + $^{144,148,154}Sm$. The dot-dashed curve is the prediction of the classical model of Bass for ^{16}O + ^{144}Sm. The dashed curves are one-dimensional model fits to the low and high energy data for ^{16}O + ^{154}Sm, respectively. They include tunnelling and define the asymptotic barrier shift D_∞, which is shown here in units of B_0. [The data are from J.R. Leigh et al., Phys. Rev. C 52 (1995) 3151.]*

spective fusion barriers B_0 as obtained from fits to the high energy data using the one-dimensional model. This removes energy shifts caused by the different sizes of the samarium nuclei. The three excitation functions merge at energies above B_0, where they are well reproduced by the prediction of the classical model of Bass, and where they can be fitted with a one-dimensional model calculation. At energies below B_0 all three excitation functions show fusion cross sections greater than zero, as would be expected to arise from tunnelling. However, the cross sections exceed by far the prediction of the one-dimensional model calculation even when tunnelling is included.

For the lightest system, ^{16}O + ^{144}Sm, it is possible[65] to obtain reasonable agreement between theory and experiment over the whole energy range by varying the potential parameters, though this reduces the quality of the fit at the higher ener-

[65]D. Abriola *et al.*, Phys. Rev. C **39** (1989) 546.

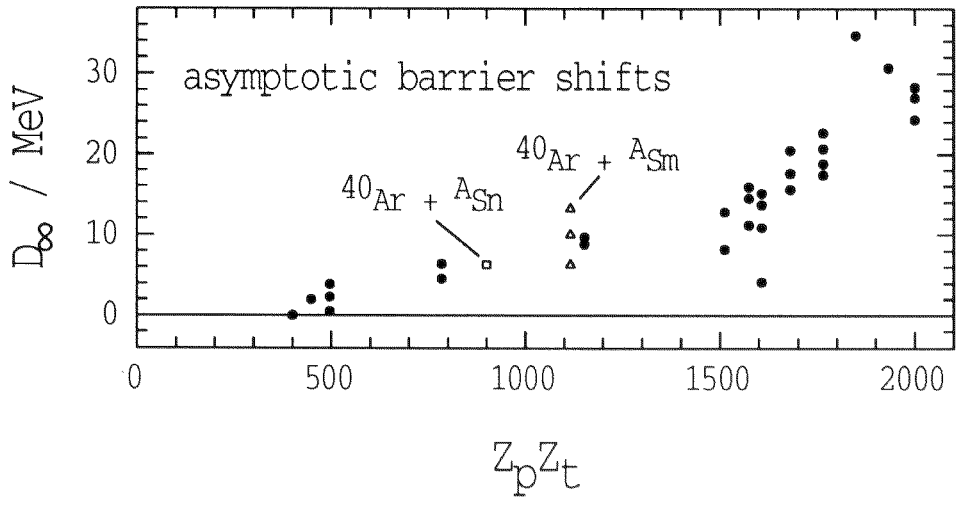

Figure 1.8: *Asymptotic energy shifts for a selection of systems as a function of Z_pZ_t. Experimental uncertainties are of the order of 10%. [The data have been adopted from A.B. Quint et al., Z. Phys. A 346 (1993) 119.]*

gies. The large sub-barrier enhancements for the other two systems can, however, not be reproduced in a one-dimensional model calculation for any set of potential parameters.

It is observed, as predicted by Equation 1.33, that asymptotically, at energies well below B_0 the excitation functions fall approximately linearly in the logarithmic representation. Thus the sub-barrier enhancement can be parametrized, as shown in Figure 1.7, in terms of the energy shift D_∞ between the linear tails of one-dimensional model calculations, which fit the high and the low energy cross sections, respectively. Such energy shifts have been extracted for many reactions and they are shown in Figure 1.8 for a selection of systems as a function of Z_pZ_t. Whereas light systems show no or small shifts, with increasing Z_pZ_t the shifts become larger and reach values $D_\infty > 20$ MeV for the heaviest systems.

It has been established[66,67] that the observed sub-barrier fusion enhancements relative to the one-dimensional model predictions are not caused by the use of incorrect sets of potential parameters in the calculations. This possibility arises, since larger fusion cross sections could be calculated, when the barriers are narrower than

[66]A.B. Balantekin, S.E. Koonin, J.W. Negele, Phys. Rev. C **28** (1983) 1565.

[67]M. Inui, S.E. Koonin, Phys. Rev. C **30** (1984) 175.

assumed. Using an inversion procedure[68] the barrier shape can be deduced from the experimental fusion cross sections assuming that there exists an energy-independent potential barrier of height B_0. For systems with $Z_pZ_t \lesssim 100$ the extracted barrier shapes differ only slightly from those resulting from the global potentials. In contrast, for the heavier systems ($Z_pZ_t \gtrsim 100$) the extracted barrier shapes are very different from the ones predicted and in many cases they are not single-valued and thus unphysical. This shows that the measured sub-barrier fusion enhancement cannot be explained by a different parametrization of the potential, but involves more complicated physics than included in the one-dimensional model.

The excitation functions in Figure 1.7 illustrate that there can be considerable variations of the sub-barrier fusion enhancement among a series of systems where one nucleus is combined with different isotopes of another element. In the case of $^{16}O + {}^{144,148,154}Sm$ the enhancement rises with increasing neutron number of the samarium isotopes[69,70]. This effect has also been observed[71] for the same series of even-even samarium isotopes when fused with ^{40}Ar, which clearly assigns the cause of the variations in enhancement to the properties of the samarium nuclei. These findings contrast sharply with results for the sequence of tin isotopes $^{112,116,122}Sn$ where no isotopic variations are observed[72,73] when they are combined with both ^{16}O and ^{40}Ar. The variations in sub-barrier fusion enhancement with nuclear charge- and mass-number are reflected in the asymptotic barrier shifts displayed in Figure 1.8. The apparently irregular dependence on charge and mass in addition to its rise with Z_pZ_t suggests that the enhancement is a nuclear structure effect. The fact that nuclei with strong rotational and vibrational states, like the samarium isotopes, show large sub-barrier fusion enhancements, identifies such collective excitations as a possible cause for the phenomenon.

The comparison of experimental excitation functions for symmetric systems reveals a second possible origin of the sub-barrier fusion enhancements[74]. To understand this, it may be assumed that the enhancement is entirely caused by the nuclear structure of the fusing nuclei. If this is presumed to occur in a way that

[68]M. Beckerman, Phys. Rep. **129** (1985) 145.

[69]R.G. Stokstad *et al.*, Phys. Rev. C **21** (1980) 2427.

[70]D.E. DiGregorio *et al.*, Phys. Lett. B **176** (1986) 322.

[71]W. Reisdorf *et al.*, Phys. Rev. Lett. **49** (1982) 1811.

[72]P. Jacobs *et al.*, Phys. Lett. B **175** (1986) 271.

[73]W. Reisdorf *et al.*, Nucl. Phys. A **438** (1985) 212.

[74]W. Reisdorf, J. Phys. G: Nucl. Part. Phys. **20** (1994) 1297.

the contributions to the enhancement of the two nuclei are independent from each other, the excitation function for the system A + B should be an average of the excitation functions for the symmetric systems A + A and B + B, where A and B represent two nuclei. This has been tested[75,76] for the isotopes ^{58}Ni and ^{64}Ni. All three possible combinations of these two isotopes show sub-barrier fusion enhancement. However, the excitation function for the asymmetric system has not been found to be an average of the two excitation functions for the symmetric system, but in fact exceeds both symmetric systems in enhancement. This result has recently been confirmed[77], although it should be noted that there are discrepancies between the newly measured excitation functions and the earlier experimental data.

The comparison of the three nickel reactions shows that a mechanism is responsible for at least part of the sub-barrier fusion enhancement, in which the two reaction partners are not independent but interact with each other. Since the asymmetry in neutron-to-proton ratio for ^{58}Ni + ^{64}Ni favours the transfer of neutrons from the heavier to the lighter isotope, it is highly suggestive, that neutron transfer, or particle transfer in general, provides such a mechanism.

Thus, from the experimental data alone, it is clear that nuclear fusion is in general not a one-dimensional problem representative of the trivial limit of the generalized barrier problem discussed in Section 1.2.3, but that it involves other degrees of freedom which couple to the relative motion across the barrier. The data suggest that the important channels among these additional degrees of freedom are associated with rotational and vibrational excitations of the nuclei and particle-transfer between the reactants.

1.4.4 Fusion Hindrance

For systems with $Z_pZ_t \lesssim 1500$ the classical model of Bass[78] reproduces the height of the fusion barrier B_0 as extracted from fits to the experimental above-barrier cross sections using the one-dimensional model, generally within 1%. In contrast, for heavier systems with $Z_pZ_t \gtrsim 1500$ the barriers extracted from the experimental data are found to be higher than the ones predicted by the Bass model. The difference in barrier height, dubbed 'extra push', can be used to parametrize this

[75]M. Beckerman *et al.*, Phys. Rev. Lett. **45** (1980) 1472.

[76]M. Beckerman *et al.*, Phys. Rev. C **23** (1981) 1581; Phys. Rev. C **25** (1982) 837.

[77]D. Ackermann, *Ph.D.-thesis*, Technische Hochschule Darmstadt, Germany (1994).

[78]R. Bass, Phys. Rev. Lett. **39** (1977) 265.

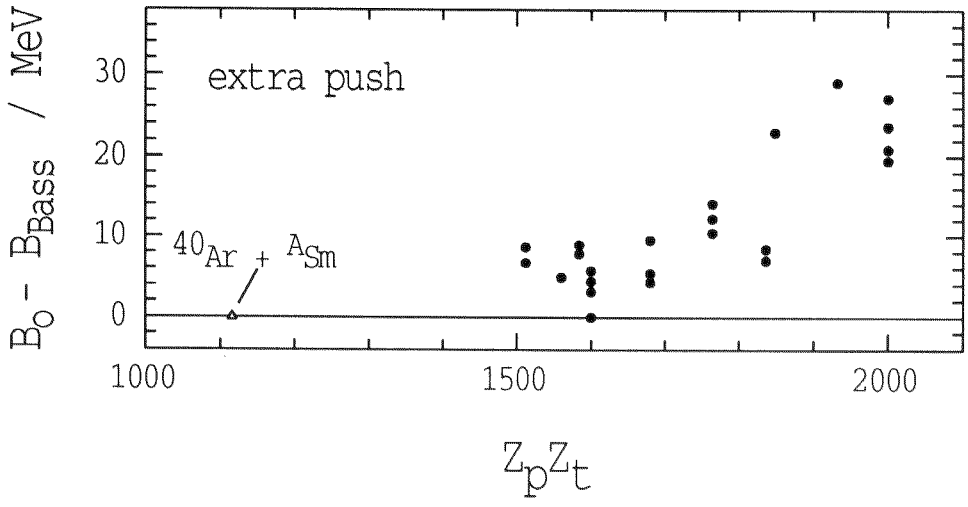

Figure 1.9: *The 'extra push' ($B_0 - B_{Bass}$) for a selection of systems as a function of Z_pZ_t. Experimental uncertainties which are of the order of a few MeV are not indicated. [The data have been adopted from A.B. Quint et al., Z. Phys. A 346 (1993) 119.]*

phenomenon of apparent fusion hindrance. The 'extra push' is shown in Figure 1.9 for a selection of reactions as a function of Z_pZ_t. It should be noted that the experimental data presented in this figure for the systems with $Z_pZ_t \gtrsim 1500$ have been deduced from evaporation residue measurements alone. Since for these reactions the compound nucleus decays dominantly via fission, the data rely on statistical model calculations. The limitations of this method have been discussed elsewhere[79,80]. However, the data can certainly be expected to show the correct trends.

In a manner similar to the asymptotic barrier shift D_∞, the 'extra push' increases with the product Z_pZ_t. It is therefore roughly a function of the size of the system. With increasing size the number of internal degrees of freedom of the system rises dramatically. In particular the number of transfer channels increases. Thus fusion may be preceded by the massive exchange of nucleons. This would have several consequences. Firstly, the potential energy is affected because of the redistribution of nucleons between projectile and target nucleus, e.g. more symmetric charge distributions result in higher fusion barriers. Secondly, the potential energy of the system is also modified by the presence of nuclear matter between the reactants, which is often referred to as a *neck-formation*. Thirdly, the system has

[79]K.H. Schmidt, W. Morawek, Rep. Prog. Phys. **54** (1991) 949.

[80]A.B. Quint *et al.*, Z. Phys. A **346** (1993) 119.

to dissipate kinetic energy to open the various, mostly negative Q-value channels. The observation of fusion hindrance has been interpreted as a signature of these effects and models have been developed which treat fusion on a multi-dimensional potential energy surface as a function of distance, mass-asymmetry, neck-formation and energy dissipation[81,82].

1.5 Multi-Dimensional Models of Fusion

The apparent failure of the one-dimensional model to give a global description of fusion demands a multi-dimensional treatment of the problem. This has been attempted phenomenologically and with models which are based on the truncation and the macroscopic limit of the generalized barrier problem. This section gives an overview of the various approaches which are of relevance in this study.

1.5.1 Geometrical Model

In a large class of nuclei the low-lying states are dominated by collective excitations of rotational character. For these nuclei the coupling of the relative motion to the rotational states may be described in the corresponding classical limit, namely as the fusion of two rigid rotors[83,84]. Compared to the time scale of the relative motion the classical rotation associated with the excitations is slow and the nuclei may be assumed to be frozen in shape and orientation during the interaction. Thus the fusion cross section depends on the mutual orientation of the nuclei with

$$\sigma^{fus}(E) = \frac{1}{16\pi^2} \int \sigma^{fus}(E, \vartheta_1, \vartheta_2) d\Omega_1 d\Omega_2 \tag{1.34}$$

where $\sigma^{fus}(E, \vartheta_1, \vartheta_2)$ is the differential cross section for a particular mutual orientation, defined by the angles ϑ_1 and ϑ_2, and the $d\Omega_i$ are the solid angle elements. The $\sigma^{fus}(E, \vartheta_1, \vartheta_2)$ are calculated by expanding the nuclear shapes in terms of spherical harmonics which yields a specific fusion radius for every orientation. For example for two prolate nuclei the fusion radius is larger when they are oriented tip-to-tip and smaller when they are oriented side-to-side. Thus the barrier is lower when

[81] W.J. Swiatecki, Phys. Scripta **24** (1981) 113.

[82] J.P. Blocki, H. Feldmeier, W.J. Swiatecki, Nucl. Phys. A **459** (1986) 145.

[83] J.O. Rasmussen, K. Sugawara-Tanabe, Nucl. Phys. A **171** (1971) 497.

[84] C.Y. Wong, Phys. Rev. Lett. **31** (1973) 766.

the tips face each other during the collision as compared to the situation where the sides face each other.

The geometrical model has been applied[85] to the fusion of ^{16}O with the series of even-A samarium isotopes $^{144-154}$Sm. These samarium isotopes undergo a shape transition with increasing neutron number from spherical to prolate deformed. This is reflected in the fusion excitation functions as an increase in sub-barrier fusion enhancement, as it is shown in Figure 1.7. While the geometrical model explains the trend of this isotopic change in fusion enhancement correctly, it overestimates the cross sections. This is presumably due to the neglect of the excitation energies[86].

Recently, the geometrical model has been used in the interpretation of the competition between fusion-fission and quasi-fission in ^{16}O + ^{238}U. Because of the larger angular momenta involved, collisions of the ^{16}O projectile with the tip of the prolate deformed ^{238}U target nucleus are suggested to lead to quasi-fission, while the more compact configuration, which occurs when the projectile collides with the side of ^{238}U, may favour fusion-fission. Such orientation effects in fusion are of particular interest in the search for new 'super-heavy' elements[87,88].

1.5.2 Barrier Distributions

The geometrical model predicts that for reactions involving rotational nuclei the one-dimensional Coulomb barrier is replaced by a continuous distribution of fusion barriers which correspond to the different mutual orientations of projectile and target nucleus. This concept can be extended[89] by assuming that the coupling to internal degrees of freedom of the binary system generally gives rise to a multitude of fusion channels which correspond to a *distribution of fusion barriers* $D(B)$. The fusion excitation function is then given by

$$\sigma^{fus}(E) = \int_0^\infty D(B)\sigma^{fus}(E,B)dB \tag{1.35}$$

where $\sigma^{fus}(E,B)$ is the fusion excitation function for the barrier B. The distribution $D(B)$ is a weighing function with

$$\int_0^\infty D(B)dB = 1 \tag{1.36}$$

[85]R.G. Stokstad, E.E. Gross, Phys. Rev. C **23** (1981) 281.

[86]P.M. Jacobs, U. Smilansky, Phys. Lett. B **127** (1983) 313.

[87]D.J. Hinde *et al.*, Phys. Rev. Lett. **74** (1995) 1295.

[88]A. Iwamoto *et al.*, Nucl. Phys. A **596** (1996) 329.

[89]P.H. Stelson, Phys. Lett. B **205** (1988) 190.

This concept has been explored for many reactions assuming continuous and symmetric distributions of rectangular or Gaussian shapes[90,91].

1.5.3 Channel Coupling

For reactions with $Z_pZ_t \lesssim 1500$ the coupling between the relative motion of the binary system and its internal degrees of freedom has been most successfully described assuming that the system represents the truncation limit of the generalized barrier problem. Thus, it is presumed that the internal degrees of freedom of the binary system, which are dominated by collective excitations and one or two nucleon transfer reactions, are few and strong. Each internal degree of freedom is associated with a particular reaction channel $j = 0, 1, .., n$ with j=0 being the elastic scattering channel. Following Equation 1.14, the coupled equations for the radial wave functions $\phi_j(r)$ of the three-dimensional system may then be written as[92,93]

$$[T + V(r) + V_{cent}(r, \ell_j) - E]\,\phi_j(r) = -\sum_{i=0}^{n} M_{ji}(r)\phi_i(r) \qquad (1.37)$$

where T is the kinetic energy operator, $V(r)$ is the interaction potential given by Equation 1.18 and $V_{cent}(r, \ell_j)$ is the centrifugal potential given by Equation 1.24. The $M_{ji}(r)$ are the elements of the coupling matrix given by Equation 1.15 and ℓ_j is the angular momentum quantum number for channel j.

Exact Numerical Solution of the Coupled Equations

As in the one-dimensional model, in the coupled-channels model the fusion cross section corresponds to the in-coming flux which overcomes the barrier. However, the wave-function is modified by the coupling interactions and the reflected flux is distributed over all the reaction channels which are associated with the internal degrees of freedom. Depending on the nature of the couplings the matrix elements $M_{ji}(r)$ may be calculated using the collective model or using a suitable model of transfer reactions[94]. The solutions of the coupled equations (1.37) may then be obtained numerically[95] by simulating loss of flux to fusion and the residual reaction

[90]H.J. Krappe *et al.*, Z. Phys. A **314** (1983) 23.

[91]A.K. Mohanty, S.K. Kataria, Pramana 43 No. 4 (1994) 319.

[92]N. Austern, *Direct Nuclear Reaction Theories*, Wiley, New York (1970).

[93]G.R. Satchler, *Direct Reactions*, Oxford University Press, Oxford (1983).

[94]I.J. Thompson, *Coupled Reaction Channels ...*, Comp. Phys. Rep. 7 (1988) 169.

[95]M.S. Melkanoff *et al.*, *Methods in Computational Physics* **6**, Academic, New York (1966).

channels not included in the coupling matrix with an imaginary volume potential $W(r)$. For large distances the wave-function has to be matched to an incident plane wave of unit norm in the entrance channel and to out-going radial waves in all exit channels[96,97]. The coefficients of the out-going waves then determine the various reaction cross sections $\sigma_j^{reac}(E)$ and conservation of flux enables the fusion cross section to be obtained from

$$\sigma^{fus}(E) = \sigma^{tot}(E) - \sum_{j=1}^{n} \sigma_j^{reac}(E) \tag{1.38}$$

where σ^{tot} is the total reaction cross section. With Equation 1.26 this can be expressed[98] in terms of the elements S_j^ℓ of the scattering matrix

$$\sigma^{fus}(E) = \pi\lambda^2 \sum_{\ell=0}^{\infty}(2\ell+1)\mathcal{T}_\ell(E) = \pi\lambda^2 \sum_{\ell=0}^{\infty}(2\ell+1)\left(1 - \sum_{j=1}^{n}|S_j^\ell|^2\right) \tag{1.39}$$

The complicated numerical calculations have been computerised. In this work the code ECIS[99] has been employed to carry out such calculations.

Simplified Solutions of the Coupled Equations

The exact coupled-channels model can be simplified[100] by introducing approximations to the treatment of the channel dependent angular momenta ℓ_j. In the iso-centrifugal approximation the centrifugal potentials $V_{cent}(r, \ell_j)$ for all channels with the same total angular momentum $J\,\hbar$ are replaced by

$$V_{cent}(r, J) = \frac{\hbar^2}{2\mu r} J(J+1) \tag{1.40}$$

This can be justified because the interactions at the barrier typically involve changes in angular momentum of only a few $\hbar$ which compares with orbital angular momenta which can be several tens of $\hbar$. The iso-centrifugal approximation which is also often referred to as no-Coriolis or orbital-sudden approximation is employed in a code[101] which has been used in this work to predict fusion excitation functions. For even-even nuclei, J may be replaced by the orbital angular momentum in the elastic

[96]B. Buck, P.E. Hodgson, Phil. Mag. **8** (1963) 1805.

[97]T. Tamura, Rev. Mod. Phys. **37** (1965) 679.

[98]G.R. Satchler, *Introduction to Nuclear Reactions*, Macmillan Press, London (1980).

[99]J. Raynal, in *Computing as a Language of Physics*, I.A.E.A Vienna (1972) 281.

[100]A.V. Andres, N. Rowley, M.A. Nagarajan, Nucl. Phys. A **481** (1988) 600.

[101]N. Rowley, A. Kruppa, *to be published.*

channel ℓ. Calculations based on the iso-centrifugal approximation are particularly suited for fusion, since the fusion cross section is not affected by this approximation. For scattering the approximations have two important consequences. The angular momentum couplings are ignored and the orbital angular momentum of the inelastic scattering and transfer channels for a certain detection angle is assumed to be equal to the angular momentum of elastic scattering at this angle. Consequently, all scattering is assumed to be *quasi-elastic.*

It is also reasonable to presume that the nuclear structure of the colliding nuclei is not disturbed until fusion occurs inside the barrier. In this case[102-106] the coupling potentials factorize with $v_i^{coup}(r,\alpha_i) = f_i(r)g_i(\alpha_i)$. The form factors $f_i(r)$ depend only on the inter-nuclear distance and the functions $g_i(\alpha_i)$ depend exclusively on the internal coordinates. Thus, the matrix elements (1.15) become

$$M_{ji}(r) = \int \chi_j^*(\alpha_j) f_i(r) g_i(\alpha_i) \chi_i(\alpha_i) d\alpha_i + \epsilon_i \delta_{ji} \tag{1.41}$$

The coupled equations (1.37) can then be de-coupled for two cases, which are known as *constant coupling* and *sudden* approximations. In the case of constant coupling the form factor is assumed to be constant with r, e.g. $f_i(r) \equiv f_0$ for all i, whereas in the sudden approximation the excitation energies of the internal degrees of freedom are ignored, e.g. $\epsilon_i \equiv 0$ for all i. In both approximations the analytical diagonalization of the matrix $M_{ji}(r)$ and the exact de-coupling of the coupled equations (1.37) is possible.

In order to achieve the de-coupling, the radial wave functions may be expressed as

$$\phi_j(r) = U_{jk} Y_k(r) \tag{1.42}$$

where U_{jk} is a unitary transformation matrix. In Equation 1.42 and in the following matrix equations Einstein's convention is applied, that summation occurs over all double indices. Inserting Equation 1.42 into Equation 1.37 yields

$$[T + V(r) + V_{cent}(r,\ell) - E]\, U_{jk} Y_k(r) = M_{ji}(r) U_{il} Y_l(r) \tag{1.43}$$

This is equivalent to

$$[T + V(r) + V_{cent}(r,\ell) - E]\, Y_k(r) = U_{kj}^{\dagger} M_{ji}(r) U_{il} Y_l(r) \tag{1.44}$$

[102] C.H. Dasso, S. Landowne, A. Winther, Nucl. Phys. A **405** (1983) 381.

[103] C.H. Dasso, S. Landowne, A. Winther, Nucl. Phys. A **407** (1983) 221.

[104] R.A. Broglia *et al.*, Phys. Rev. C **27** (1983) 2433; Phys. Lett. B **133** (1983) 34.

[105] P.M. Jacobs, U. Smilansky, Phys. Lett. B **127** (1983) 313.

[106] R. Lindsay, N. Rowley, J. Phys. G: Nucl. Part. Phys. **10** (1984) 805.

where the dagger indicates Hermitean conjugation. The unitary transformation U_{jk} may be chosen, so that it diagonalizes the coupling matrix $M_{ji}(r)$ and

$$U^{\dagger}_{kj} M_{ji}(r) U_{il} = b_k \delta_{kl} \tag{1.45}$$

where the b_k are the eigen-values. Then, the coupled equations (1.37) de-couple to yield a system of uncoupled Schrödinger equations for the wave functions $Y_k(r)$

$$\left[T + V(r) + V_{cent}(r,\ell) - E + b_k\right] Y_k(r) = 0 \tag{1.46}$$

The constant coupling approximation can be relaxed by introducing[107] a radial dependence for the eigen-values b_k and expanding $V(r) + b_k(r)$ in the region around B_0. This improves the accuracy of the model considerably.

The de-coupled equations (1.46) may be solved with the eigen-functions $\bar{Y}_k(r)$ which correspond to the eigen-channels $k = 0, 1, .., n$. The eigen-functions have to fulfil the boundary condition (1.27) that for large distances there is an in-going plane wave of unit norm in the entrance-channel and that there are out-going radial waves in all exit-channels. In order to comply with the same boundary conditions for the radial wave-functions $\phi_j(r)$ of the actual reaction channels, the functions $Y_k(r)$ in the expansion 1.42 have to be chosen as $Y_k(r) = U_{0k}\bar{Y}_k(r)$. Then the radial wave functions are given by

$$\phi_j(r) = U_{jk} U_{0k} \bar{Y}_k(r) \tag{1.47}$$

Consequently, the elements of the scattering matrix for the physical reaction channels ($j = 1, .., n; j \neq 0$) are

$$S^{\ell}_j = U_{jk} U_{0k} \bar{S}^{\ell}_k \tag{1.48}$$

where the $\bar{S}^{\ell}_k$ are the elements of the scattering matrix for the eigen-channels. With Equation 1.39 it follows that

$$\sigma^{fus}(E) = \pi\lambda^2 \sum_{\ell,j,k,l} (2\ell+1) \left(1 - U_{jk} U_{0k} \bar{S}^{\ell}_k U^{*}_{jl} U^{*}_{0l} \bar{S}^{\ell *}_l\right). \tag{1.49}$$

Using the relation

$$U_{jk} U^{*}_{jl} = U^{\dagger}_{lj} U_{jk} = \delta_{kl} \tag{1.50}$$

Equation 1.49 reduces to

$$\sigma^{fus}(E) = \pi\lambda^2 \sum_{\ell,k} W_k (2\ell+1)(1 - |\bar{S}^{\ell}_k|^2) = \sum_k W_k \sigma^{fus}\left(E, V(r) + b_k\right) \tag{1.51}$$

[107] C.H. Dasso, S. Landowne, Phys. Lett. B **183** (1987) 141.

where the $W_k \equiv |U_{0k}|^2$ are the weights with which the various eigen-channels contribute to the fusion cross section. This requires that $\sum_{k=0}^{n} W_k = 1$. Each eigen-channel can be associated with a potential $V(r)+b_k$ which forms a potential barrier of height $B_k = V(R_0) + b_k$ at the inter-nuclear distance R_0. This interpretation is referred to as the *eigen-channel model.*

Thus, the channel coupling replaces the one-dimensional Coulomb barrier $B_0 \equiv V(R_0)$ with a spectrum of $n+1$ potential barriers which are weighted with the factors W_k. This distribution of potential barriers is given by

$$D(E, B_k) \equiv W_k \delta(E - B_k) \quad \text{for } k = 0, 1, .., n \tag{1.52}$$

It can be shown, that there is always at least one negative eigen-value b_k resulting in a barrier which is lower than the one-dimensional Coulomb barrier. It follows, that it is fusion over the low energy barriers which is responsible for the sub-barrier fusion enhancement.

The simplified solution of the coupled-channels equations described in the preceding paragraphs is the basis of the computer code CCMOD[108]. CCMOD is a modified version of the code CCDEF[109,110] and performs the diagonalization of the coupling matrix $M_{ji}(r)$ numerically at each value of the inter-nuclear distance r. It does, however, not include the full dynamical effects of the finite excitation energies. In CCMOD the coupling to vibrational or rotational excitations is estimated from the collective model expression, so that the matrix elements are

$$M_{ji}(r) = \frac{\beta_{ji}}{\sqrt{4\pi}} \left[-R_a \frac{dV(r)}{dr} + \frac{3 Z_p Z_t e^2}{(2\lambda_{ji}+1)} \frac{R_a^{\lambda_{ji}}}{r^{\lambda_{ji}+1}} \right] - Q_j \delta_{ji} \tag{1.53}$$

where β_{ji} is the deformation parameter associated with the transition from channel j to channel i and λ_{ji} is its multipolarity. The radius of the excited nucleus is R_a and the $Q_j \equiv -\epsilon_j$ are the Q-values.

Coupling to transfer reactions can be included approximately[111] with the matrix elements

$$M_{ji}(r) = \frac{F_{ji}}{\sqrt{4\pi}} \exp\left[\frac{R_a^{(p)} + R_a^{(t)} - r}{a_{tr}} \right] - Q_j \delta_{ji} \tag{1.54}$$

where $R_a^{(p,t)}$ are the nuclear radii, F_{ji} is the coupling strength, which is often referred to as F_0, a_{tr} is a suitable diffuseness parameter and Q_j is the transfer Q-value. The

[108] M. Dasgupta *et al.*, Nucl. Phys. A **539** (1992) 351.

[109] C.H. Dasso, S. Landowne, Comp. Phys. Comm. **46** (1987) 187.

[110] J. Fernández Niello, C.H. Dasso, S. Landowne, Comp. Phys. Comm. **54** (1989) 409.

[111] R.A. Broglia *et al.*, Phys. Lett. B **133** (1992) 34.

quantities F_{ji} and a_{tr} can vary considerably depending on the transferred angular momentum and the nucleon orbitals involved in the transfer process[112].

Because of its great simplicity, the code CCMOD is a valuable tool for analyzing fusion excitation functions, provided one keeps its limitations in mind. The code is particularly useful for judging the relative importance of different couplings.

Experimental Determination of the Barrier Distribution

When it is assumed that the contribution to the fusion cross section from each barrier B_k is given by the classical formula 1.32 and that each barrier is located at the same inter-nuclear separation R_0, the transmission coefficient can be recovered from the fusion excitation function[113]

$$T(E) = \frac{1}{\pi R_0^2}\frac{d}{dE}\left[E\sigma^{fus}(E)\right] \tag{1.55}$$

Consequently further differentiation with respect to energy yields the barrier distribution (1.52), since[114]

$$\frac{1}{\pi R_0^2}\frac{d^2}{dE^2}\left[E\sigma^{fus}(E)\right] = \frac{d^2}{dE^2}\left[\sum_{k=0}^{n} W_k(E-B_k)\right] = W_k\delta(E-B_k) \equiv D(E,B_k) \tag{1.56}$$

This is illustrated in Figure 1.10 for two barriers with weights 0.4 and 0.6, respectively. In the classical approximation the function $E\sigma^{fus}(E)$ is a superposition of two straight lines and there is no fusion at energies below the lowest barrier. Consequently, the first differential with respect to energy of $E\sigma^{fus}(E)$ is a step-function. The second differential with respect to energy then yields δ-functions at the energies B_k which are weighed with $(\pi R_0^2 \times W_k)$. The second differential is thus equivalent to the barrier distribution $D(E, B_k)$.

When tunnelling is included, the fusion cross sections for a single barrier B_k are approximately given by Equation 1.31. Double differentiation of $E\sigma^{fus}(E)$ with respect to energy then yields

$$\frac{1}{\pi R_0^2}\frac{d^2}{dE^2}\left[E\sigma^{fus}(E)\right] = \left[\left(\frac{2\pi}{\hbar\omega_0}\right)\frac{e^x}{(1+e^x)^2}\right] \equiv G^{fus}(E,B_k) \tag{1.57}$$

where $x \equiv (2\pi/\hbar\omega_0)(E-B_k)$ and $G^{fus}(E,B_k)$ is a peaked function. It follows that the second differential of the fusion excitation function for a distribution of barriers

[112]G. Pollarolo, R.A. Broglia, A. Winther, Nucl. Phys. A **406** (1983) 369.

[113]A.B. Balantekin, P.E. Reimer, Phys. Rev. C **33** (1986) 379.

[114]N. Rowley, G.R. Satchler, P.H. Stelson, Phys. Lett. B **254** (1991) 25.

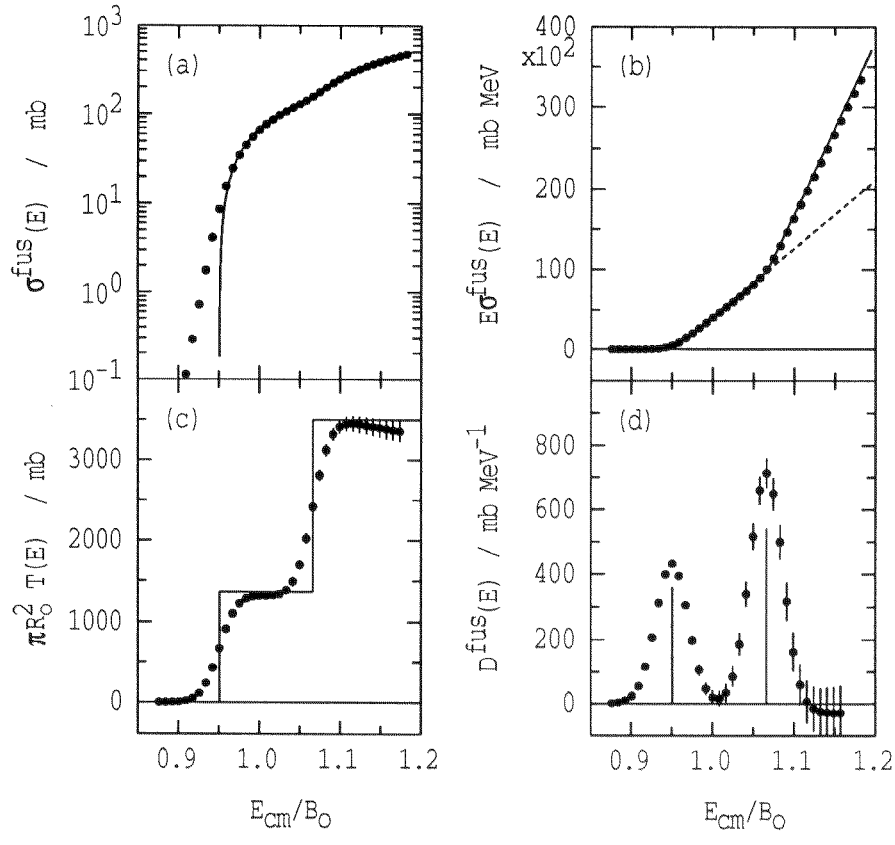

Figure 1.10: *Experimentally, the structure of the barrier distribution $D(E, B_k)$ can be extracted from the excitation function by double differentiation of $E\sigma^{fus}(E)$. This is demonstrated for two barriers with weights 0.4 and 0.6, respectively. The solid curves are the classical limit, while the points, which have been calculated including tunnelling, represent a hypothetical data-set with relative uncertainties of 1%. (a) The fusion excitation function. (b) The function $E\sigma^{fus}(E)$. (c) The first differential of $E\sigma^{fus}$ with respect to energy, which is proportional to the transmission function $T(E)$. (d) The representation $D^{fus}(E)$ of the barrier distribution. The energy scales have been divided by an arbitrary B_0.*

B_k is given by

$$\frac{d^2}{dE^2}\left[E\sigma^{fus}(E, B_k)\right] = \pi R_0^2 \sum_{k=0}^{n} W_k G^{fus}(E, B_k) \equiv D^{fus}(E) \qquad (1.58)$$

Comparison with Equation 1.56 shows that the distribution $D^{fus}(E)$ is a representation of the barrier distribution $D(E, B_k)$.

The functions $G^{fus}(E, B_k)$ satisfy $\int G^{fus}(x)dx = 1$ and they become δ-functions in the limit $\hbar\omega_0 \to 0$. The full width at half maximum of $G^{fus}(E, B_k)$ is

$$\Delta E_{FWHM} = 0.56\hbar\omega_0 \approx 2 - 3 \text{ MeV} \qquad (1.59)$$

Thus, for barrier distributions where the differences in barrier height are comparable to 2–3 MeV, $D^{fus}(E)$ resolves the individual barriers. However, even when the differences in barrier height are smaller, the function $D^{fus}(E)$ contains some information about the barrier distribution it represents.

The extraction of the barrier distribution representation $D^{fus}(E)$ is illustrated in Figure 1.10 for a hypothetical excitation function. The excitation function has been obtained by summing the excitation functions of two barriers calculated with Equation 1.31 using the weights 0.4 and 0.6, respectively. In Figure 1.10(a) in contrast to its classical limit, this excitation function is, as a result of tunnelling, greater than zero at the lowest energies. In Figure 1.10(c) the tunnelling smoothes the discrete steps of the classical limit. As a consequence, the distribution $D^{fus}(E)$ in Figure 1.10(d) features two peaks with finite width. The positions and integrals of these peaks are representative of the barrier heights B_k and weights W_k, respectively. The decreasing slope and the negative curvature of $E\sigma^{fus}(E)$ at the highest energies are a consequence of the decrease in barrier radius with increasing angular momentum.

In order to simulate an experimental data-set, the more realistic excitation function in Figure 1.10 is shown in discrete steps with error bars corresponding to a hypothetical relative uncertainty of 1%. In the case of experimental data the derivatives cannot be obtained analytically, but they have to be approximated with point-difference formulae. For the second differential with respect to energy of $E\sigma^{fus}(E)$ the point-difference formula is given by

$$D^{fus}(E) \simeq \frac{E\sigma^{fus}(E+\Delta E) - 2E\sigma^{fus}(E) + E\sigma^{fus}(E-\Delta E)}{(\Delta E)^2}. \tag{1.60}$$

where ΔE is the energy step length. Obviously, a small energy step ΔE approximates the analytical derivative better than a large one and increases the sensitivity to the barrier structure. However, for a fixed relative experimental uncertainty δ of the cross sections, the absolute experimental uncertainty of $D^{fus}(E)$ is approximately

$$\Delta D^{fus} \simeq \delta\sqrt{6}\frac{E\sigma^{fus}}{(\Delta E)^2}. \tag{1.61}$$

Thus, ΔD^{fus} increases with energy and cross section, as seen in Figure 1.10(d). Increasing the step length ΔE reduces ΔD^{fus} and improves the precision of the data. It follows that a compromise has to be found between sensitivity and precision. The optimum information about the barrier distribution can be gained from the

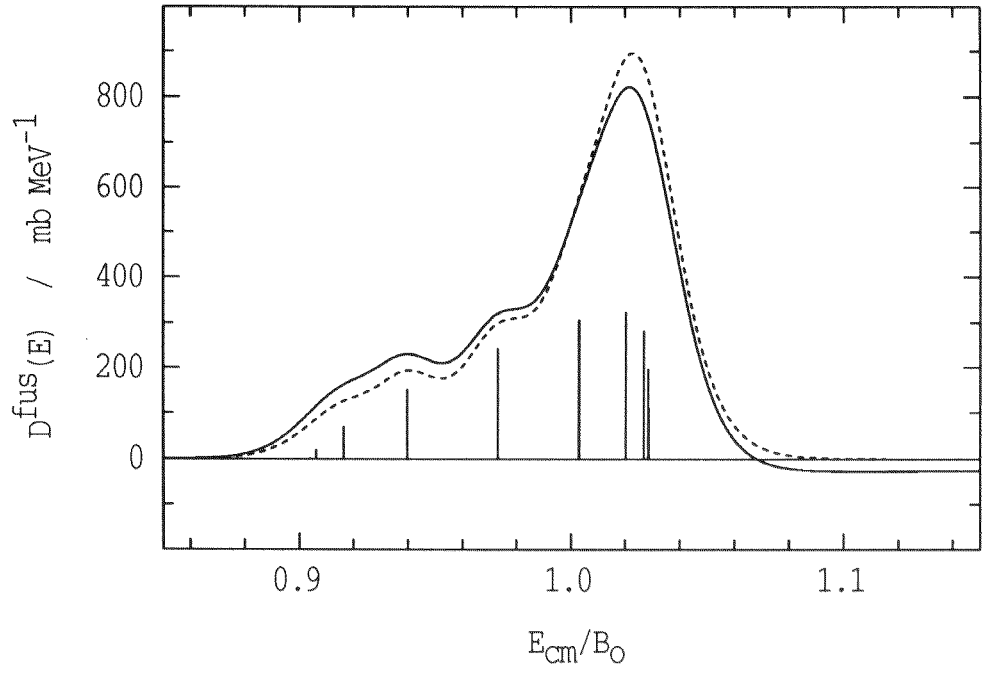

Figure 1.11: *The barrier distribution $D(E, B_k)$ for the fusion of a spherical with a deformed nucleus compared with its representations $D^{fus}(E)$ as extracted from calculations which assume a constant radius for all barriers and angular momenta (dashed) and include the changes in radius with barrier and angular momentum (solid), respectively. $D(E, B_k)$ is shown as vertical bars, whose heights represent the weights W_k. The energy scale has been divided by B_0.*

experimental data when $D^{fus}(E)$ is extracted for different values of ΔE ranging from the smallest possible to large energy steps of the order of the width of the barrier distribution itself.

The formalism presented above is only strictly valid in the eigen-channel model of fusion which results from simplified solutions of the coupled-channels equations. This approach ignores that different fusion barriers can have different fusion radii. It might therefore be argued that the barrier structure may not be present in true excitation functions. However, it has been found that this argument is not justified. Representations $D^{fus}(E)$ extracted from true excitation function retain the barrier structure predicted by the eigen-channel model. This is demonstrated in Figure 1.11. A reaction involving a spherical and a deformed nucleus with ten discrete barriers is considered. Classically the curvature of $E\sigma^{fus}$ yields a set of δ-functions. Whilst the position of a δ-function represents the height of a barrier,

its integral corresponds to the barrier weight. In Figure 1.11 the δ-functions are shown as vertical lines and the weights of the barriers are represented by the heights of the lines. When quantum mechanical penetration of the barriers is included the curvature becomes a continuous function of energy, as shown by the dashed curve in Figure 1.11. If the barrier distribution is assumed to result from deformation, then the barrier radius is different for each barrier. It is also angular momentum dependent. Including these effects results in a more realistic calculation of $D^{fus}(E)$ which is shown as solid curve in Figure 1.11. It is apparent that this calculation of $D^{fus}(E)$ is an excellent representation of the barrier structure and that the variations in barrier radius have only a small effect on this representation.

The advantages of displaying fusion excitation functions as $D^{fus}(E)$ are shown in Figure 1.12. Independent of its physical origin, the result of channel coupling is always an enhancement of the fusion cross section at low energies. From the excitation function it can hardly be distinguished, whether the effect is caused by a positive Q-value transfer channel, a negative Q-value vibrational excitation or by coupling to a band of rotational states. In contrast, the distributions $D^{fus}(E)$ display clear signatures of the different coupling schemes and, if determined to high precision, enable an unambiguous identification of those.

Barrier distribution representations $D^{fus}(E)$ have been extracted from precisely measured fusion excitation functions for several systems[115-119]. Figure 1.13 shows three cases of channel coupling which have been distinguished using experimental representations of the barrier distribution. The coupling schemes can be identified by comparison with Figure 1.12. In the reaction $^{16}O + ^{144}Sm$, the elastic channel couples to vibrational excitations of the lowest 2^+ and 3^- states of ^{144}Sm with the octupole state being dominant. The reaction $^{40}Ca + ^{40}Ca$ is a textbook example of the trivial limit of the barrier problem, i.e. coupling of the elastic channel to others is negligible. This is a consequence of the double shell closure in ^{40}Ca. For $^{16}O + ^{154}Sm$ the representation $D^{fus}(E)$ identifies couplings of the relative motion to the ground state rotational band of the prolate deformed ^{154}Sm.

The representation of fusion excitation functions as $D^{fus}(E)$ has yielded some surprising evidence for the importance of multi-phonon excitations in fusion. For

[115]J.X.Wei *et al.*, Phys. Rev. Lett. **67** (1991) 3368.

[116]R.C. Lemmon *et al.*, Phys. Lett. B **316** (1993) 32.

[117]J.R. Leigh *et al.*, Phys. Rev. C **47** (1993) R437.

[118]C.R. Morton *et al.*, Phys. Rev. Lett. **72** (1994) 4074.

[119]J.R. Leigh *et al.*, Phys. Rev. C **52** (1995) 3151.

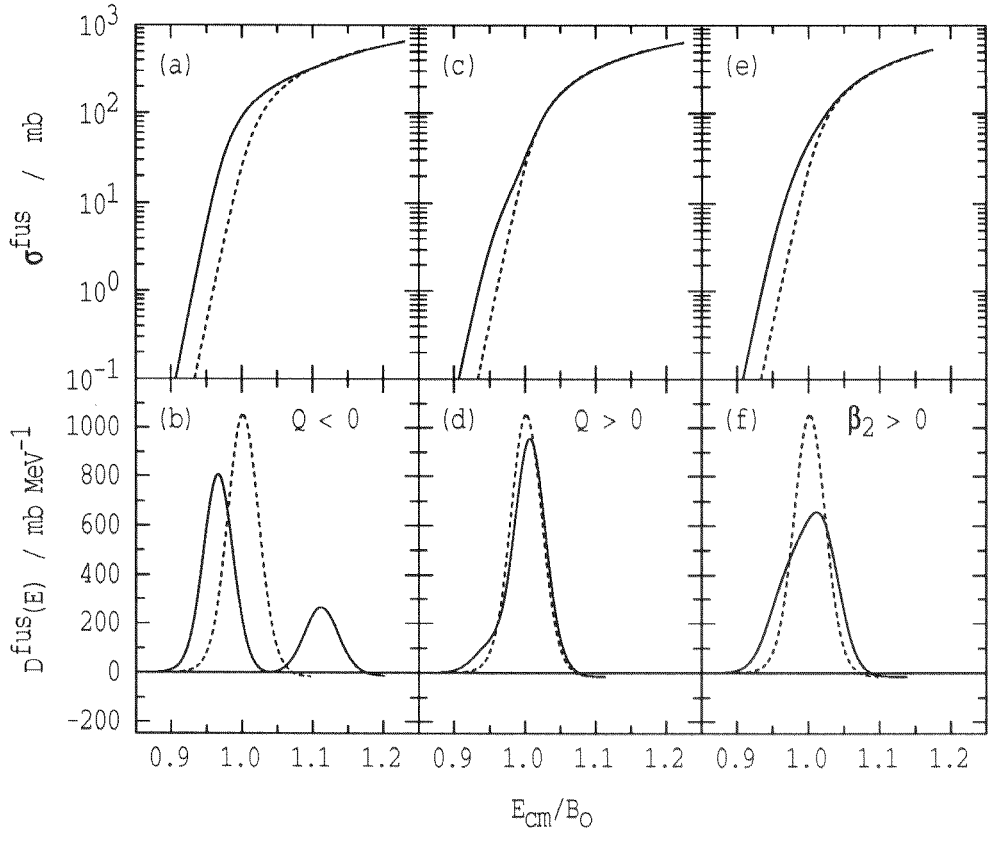

Figure 1.12: *Calculated excitation functions $\sigma^{fus}(E)$ and barrier distribution representations $D^{fus}(E)$ for different coupling schemes. The dashed curves are predictions of the one-dimensional model. The solid curves are coupled-channels calculations using* CCMOD. *The three coupling schemes shown are (a,b) coupling to a negative Q-value channel, (c,d) coupling to a positive Q-value channel, and (e,f) coupling to a series of rotational states of a prolate deformed nucleus with the deformation parameter $\beta_2 > 0$, respectively. The energy scales have been normalized by B_0. The coupling schemes can be distinguished more easily by comparing the distributions $D^{fus}(E)$ rather than the excitation functions.*

the systems ^{16}O, ^{28}Si + ^{208}Pb the experimental distributions $D^{fus}(E)$ cannot be explained with coupling schemes which include only single phonon coupling of vibrational states. It has been shown[120,121] with simplified coupled-channels calculations that the inclusion of additional coupling to an octupole double phonon state of ^{208}Pb in the calculation improves the agreement with the data considerably. This is consistent with recent spectroscopic evidence[122] for such an octupole double phonon

[120]C.R. Morton *et al.*, Phys. Rev. C **52** (1995) 243.

[121]D.J. Hinde *et al.*, Nucl. Phys. A **592** (1995) 271.

[122]M. Yeh *et al.*, Phys. Rev. Lett. **76** (1996) 1208.

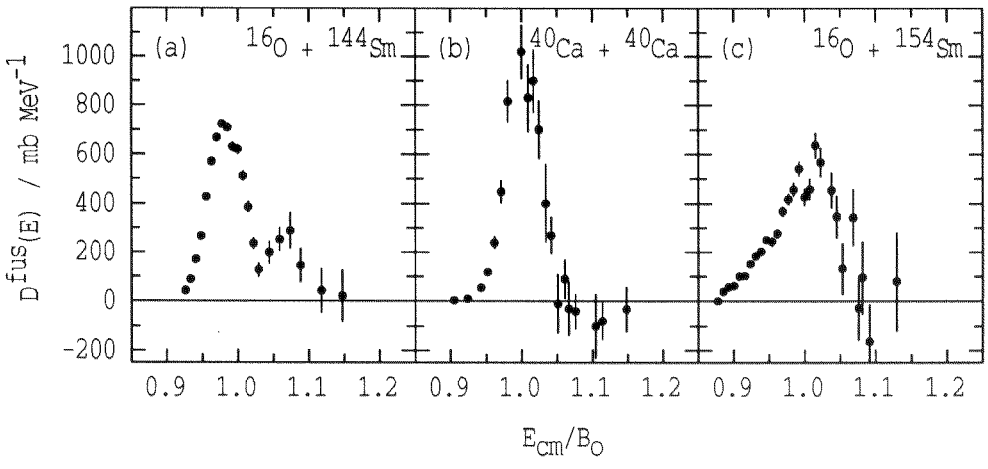

Figure 1.13: *Barrier distribution representations $D^{fus}(E)$ extracted from precisely measured fusion excitation functions display signatures of the coupling schemes involved. This is shown, (a) for the system $^{16}O + ^{144}Sm$, where coupling to the lowest vibrational octupole state is important, (b) for $^{40}Ca + ^{40}Ca$, where apparently no coupling occurs, and (c) for $^{16}O + ^{154}Sm$, where the relative motion couples to the ground state rotational band of ^{154}Sm. The energy scales have been normalized by B_0.*

state in ^{208}Pb. Furthermore, for the reaction ^{58}Ni + ^{60}Ni it has been found[123] that in the interpretation of $D^{fus}(E)$, in addition to the individual double phonon excitations of the lowest energy quadrupole phonons in both nuclei, also the mutual excitations of the double phonon states have to be taken into account. In this case there is only limited spectroscopic evidence for the existence of such states. Another encouraging result of the new technique has been the unambiguous identification of the coupling to transfer channels in the fusion of some systems[124,125].

The potential of representing fusion data as $D^{fus}(E)$ has as yet not been fully exploited. It can be hoped, that this approach to fusion will reveal even more details, when it is applied to increasingly more reactions and a complete picture emerges.

---

[123]A.M. Stefanini *et al.* Phys. Rev. Lett. **74** (1995) 864.

[124]C.R. Morton *et al.*, Phys. Rev. Lett. **72** (1994) 4074.

[125]A.M. Stefanini *et al.* Phys. Rev. C **52** (1995) R1727.

1.5.4 Neutron-Flow and Neck-Formation

It has been proposed[126,127] in a schematic model that the flow of neutrons between the colliding nuclei may precede and initiate fusion. This effect could result in a flat barrier distribution where the lowest barrier corresponds to the lowest centre-of-mass energy for which the distance of closest approach allows neutrons to flow between the potential wells of the two nuclei[128].

These speculations have encouraged the development of the neck-formation model[129,130] which is intermediate between the truncation and the macroscopic limit of the generalized barrier problem. In this model the nuclei are treated as macroscopic spheroids on a potential energy surface which depends on the inter-nuclear separation and the deformation of the nuclei. It is assumed that the deformation in the direction of the relative motion, which eventually leads to the formation of a neck[131] between the reactants, is the most important degree of freedom of the nuclear binary system apart from the relative motion itself. Thus the coupling between these two degrees of freedom is considered explicitly. In contrast to the coupled-channels model, which is based on solutions of the stationary Schrödinger equation, the neck-formation model involves the solution of the time-dependent Schrödinger equation. Consequently this model has the attractive feature of providing a history of the in-coming wave-packet as it moves over the potential energy surface.

It has been found for the system ^{58}Ni + ^{58}Ni that the fusion excitation function can be well reproduced with the neck-formation model. The important result is that the transmitted flux corresponds predominantly to trajectories which involve large deformations of the nuclei in the direction of relative motion and thus neck-formation. Since the calculations are extensive, a generalization of the model to asymmetric systems is beyond the capacity of present electronic computing power. In any case the large isotopic variations of the fusion enhancement will be difficult to address with this model, since it includes only one additional degree of freedom which is expected to vary smoothly with system size.

---

[126]P.H. Stelson, Phys. Lett. B **205** (1988) 190.

[127]P.H. Stelson *et al.*, Phys. Rev. C **41** (1990) 1584.

[128]W. von Oertzen *et al.*, Z. Phys. A **326** (1987) 463.

[129]J. Schneider, H.H. Wolter, Z. Phys. A **339** (1991) 177.

[130]C.E. Aguiar *et al.*, Nucl. Phys. A **500** (1989) 195.

[131]H.J. Krappe *et al.*, Z. Phys. A **314** (1983) 23.

1.5.5 Dissipation during Fusion

The increase in fusion hindrance with rising Z_pZ_t, as it is shown in Figure 1.9, suggests that among other effects large energy dissipation may occur in the fusion of heavy systems ($Z_pZ_t \gtrsim 1500$). This would be the consequence of weak couplings to many internal degrees of freedom such as the large number of transfer channels which are available in these heavy systems. Among other theories[132], the surface friction model[133–135], which corresponds to the macroscopic limit of the generalized barrier problem, has been employed to describe the fusion of heavy systems. The surface friction model is based on Monte Carlo calculations using the Langevin equation (1.8). By sampling trajectories a distribution function is created from which the fusion cross sections $\sigma_l^{fus}(E)$ can be obtained.

The surface friction model reproduces well the average trend of the 'extra push' energies with increasing system size. Individual deviations from the data may be attributed to nuclear structure effects which are not included in the model. The quality of the agreement is demonstrated in Figure 1.14. In this figure the 'extra push' energies are plotted as a function of the effective fissility[136]

$$x_e = \frac{4Z_pZ_t[1 - 1.7826(1 - 2Z_c/A_c)^2]}{50.883[A_p^{1/3}A_t^{1/3}(A_p^{1/3} + A_t^{1/3})]} \tag{1.62}$$

which is a more accurate quantification of the heaviness of the binary system than Z_pZ_t. The symbols Z_c and A_c represent the charge and mass numbers of the combined system, respectively.

1.6 Reflection at the Barrier

The residual of the in-going flux, which is not transmitted through a potential barrier, is reflected. This reflected flux can be quantified in terms of the differential scattering cross section $d\sigma^{qel}(E)$ which is determined from the boundary condition (1.27) of the wave function $\Psi(r)$. The index '*qel*' refers to *quasi-elastic scattering* which comprises elastic and inelastic scattering and reactions involving the transfer of a few nucleons between the surfaces of the reactants.

[132] J.P. Blocki, H. Feldmeier, W.J. Swiatecki, Nucl. Phys. A **459** (1986) 145.

[133] D.H.E Gross, L. Satpathy, Phys. Lett. B **110** (1982) 31.

[134] P. Fröbrich, Phys. Rep. **116** (1984) 337.

[135] J. Marten, P. Fröbrich, Nucl. Phys. A **545** (1992) 854.

[136] S. Bjornholm, W.J. Swiatecki, Nucl. Phys. A **391** (1982) 471.

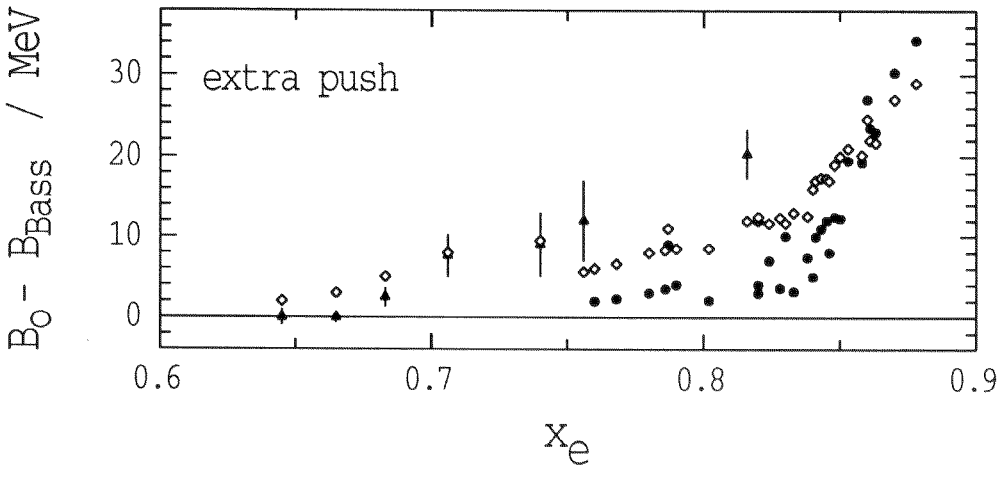

Figure 1.14: *Measured 'extra push' energies (filled triangles and circles) compared with predictions of the surface friction model (open diamonds) as a function of the effective fissility x_e. The triangles and circles represent two different series of experiments. The experimental uncertainties of the circles are a few MeV. [The figure has been adopted from P. Fröbrich, New Trends in Nuclear Collective Dynamics, Conf. Proc., to be published in Lecture Notes in Physics.]*

1.6.1 Quasi-Elastic Scattering

Quasi-elastic scattering reactions[137] are assumed to follow approximately the elastic scattering trajectories. Thus changes in kinetic energy and angular momentum during the interaction are ignored. The differential quasi-elastic scattering cross section at the scattering angle θ is given by

$$\frac{d\sigma^{qel}}{d\Omega}(E,\theta) \equiv d\sigma^{qel}(E,\theta) = |f^{qel}(E,\theta)|^2 = \sum_{j=0}^{n} |f_j(E,\theta)|^2 \qquad (1.63)$$

where $f^{qel}(E,\theta)$ is the quasi-elastic scattering amplitude and the $f_j(E,\theta)$ are the scattering amplitudes in each scattering channel with j=0 indicating the elastic channel. It should be noted that limiting the reflected flux to quasi-elastic scattering is a restriction of the general situation. For the purpose of this study, which concentrates on centre-of-mass energies of the order of the Coulomb barrier energy, this is a sensible approximation.

The scattering amplitudes $f_j(E,\theta)$ can be de-composed into contributions cor-

[137]K.E. Rehm, Ann. Rev. Nucl. Part. Sci. **41** (1991) 429.

responding to the angular momenta ℓ, so that[138,139]

$$f_j(E,\theta) = \frac{i\lambda}{2}\sum_{\ell=0}^{\infty}(2\ell+1)P_\ell(\cos\theta)\delta_{j0} + \frac{\lambda}{2i}\sum_{\ell=0}^{\infty}(2\ell+1)P_\ell(\cos\theta)\exp[2i\sigma_j^\ell(E)]S_j^\ell(E) \tag{1.64}$$

where i is the complex unit, λ is the reduced de Broglie wave length, and the $P_\ell(\cos\theta)$ are Legendre polynomials. The first term in this equation contributes only in the elastic channel. The information about the interactions is contained in the complex scattering matrix elements $S_j^\ell(E)$ and in the Coulomb phases $\sigma_j^\ell(E)$. For elastic scattering (j=0), in the absence of any other reaction channels, one obtains the Rutherford scattering amplitude

$$f_0^R(E,\theta) = \frac{i\lambda}{2}\sum_{\ell=0}^{\infty}(2\ell+1)P_\ell(\cos\theta)\left\{1-\exp[2i\sigma_0^\ell(E)]\right\} \tag{1.65}$$

and the corresponding Rutherford scattering cross section

$$d\sigma^R(E,\theta) = \frac{n^2\lambda^2}{4}\csc^4\left(\frac{\theta}{2}\right) \tag{1.66}$$

In this equation n is the Sommerfeld parameter with

$$n = \frac{\alpha Z_p Z_t}{v/c} \tag{1.67}$$

where α is the fine structure constant and v/c is the relative velocity of the nuclei for $r \to +\infty$ divided by the velocity of light.

At energies well below the Coulomb barrier the reactants do not come close enough to reach the interaction zone, so that they are neither affected by the short-range nuclear interactions nor by strong electro-static forces. Thus the differential scattering cross section is purely elastic and $d\sigma^{qel}(E,\theta)$ is identical to $d\sigma^R(E,\theta)$. Since $d\sigma^R(E,\theta)$ can be calculated exactly using Equation 1.66, it is common to use it as a normalization for nuclear scattering. Nuclear scattering occurs when the two nuclei enter the interaction zone.

The transition from Rutherford scattering to nuclear scattering takes place within a narrow region at the edge of the interaction zone. Inside this zone, which extends not far beyond the radius of the nuclear potential R_n, the nuclear forces dominate and most of the in-going flux is removed from the elastic channel.

---

[138]N.F. Mott, H.S. Massey, *The Theory of Atomic Collisions*, Clarendon Press, Oxford (1949).

[139]R. Bass, *Nuclear Reactions with Heavy Ions*, Springer, Berlin (1980).

The strong absorption in the interaction zone is the justification for the optical model of nuclear reactions which has been presented in Section 1.4.2. As in optics, for de Broglie wave lengths $\lambda \simeq R_n$, the strong absorption results in diffraction effects[140,141]. These effects are observed in the excitation functions and the angular distributions of elastic and quasi-elastic scattering.

If $n < 1$ and $E_{cm} \gg B_0$, the effect of the Coulomb repulsion between projectile and target nucleus is small. The in-going waves remain approximately plane waves until they reach the interaction zone. The absorption in the interaction zone then merely "cuts a circular piece out of the wave". This results in a diffraction pattern which is known as *Fraunhofer diffraction*. In *Fresnel diffraction*, which occurs when $n > 1$ and E_{cm} is close to B_0, the effect of the Coulomb repulsion is strong and the in-going waves diverge before they reach the interaction zone. Fresnel diffraction results in a sharp fall of the excitation function at a certain bombarding energy which can be related to the height of the potential barrier. For bombarding energies lower than this energy, the excitation function oscillates about the cross section predicted by Rutherford's formula (1.66). For inelastic scattering and transfer reactions similar diffraction effects are observed.

The importance of diffraction effects for the quasi-elastic scattering of a particular binary system can be assessed from the phenomenological diffraction diagram shown in Figure 1.15. The occurrence of diffraction and its properties depend on the Sommerfeld parameter n and the relative energy E_{cm}. For low energies no absorption occurs, so that diffraction is not observed and the nuclei follow classical trajectories. For energies larger than the one-dimensional barrier B_0 and a Sommerfeld parameter $n > 1$ absorption from the elastic channel causes Fresnel diffraction. The non-diffractive and the diffractive regimes are separated in the figure by the thick dashed curve. This curve corresponds to a grazing angular momentum $\ell_{gr}\hbar = 10\hbar$. The term 'grazing' refers to the situation where the nuclei just touch.

For large values of the pattern parameter

$$p = \frac{2n}{1 + (n/\ell_{gr})^2} \tag{1.68}$$

the de Broglie wave length is very much smaller than the dimensions of the interaction zone. This is equivalent to the limiting case of geometrical optics where

[140]W.E. Frahn, Treatise on Heavy Ion Science, Vol. 1, Plenum Press, NY (1984) 135.

[141]W.E. Frahn, *Diffractive Processes in Nuclear Physics*, Clarendon, Oxford (1985).

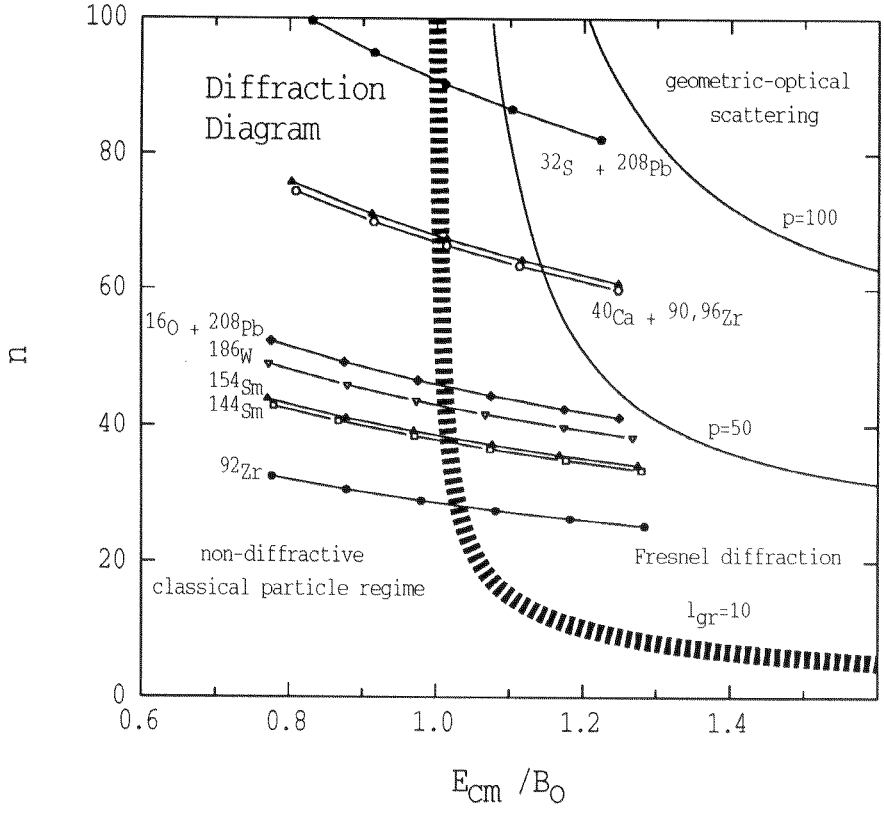

Figure 1.15: *Diffraction properties of nuclear reactions as a function of Sommerfeld parameter n and energy E_{cm}. The diffraction properties of the reactions studied in this work are indicated by the connected symbols.*

diffraction effects are negligible. Consequently, for very large n and large p the nuclei follow almost classical trajectories.

1.6.2 Unification of Fusion and Scattering Theory

The understanding of sub-barrier fusion enhancement as a phenomenon which depends on the internal degrees of freedom of the binary system challenges the traditional approach to nuclear reactions, which describes quasi-elastic scattering and fusion with two unrelated formalisms. Traditionally quasi-elastic scattering is treated as a 'microscopic' process[142] within the frame-work of the Distorted-Wave-Born-Approximation and coupled-channels theories, whereas fusion is considered a

[142]see e.g. Treatise on Heavy Ion Science, Vol. 1, Plenum Press, NY (1984).

'macroscopic' process[143], which does not depend on the nuclear structure, but only on the mass, charge and the shape of the reactants. It is now obvious from the experimental data, that the dynamics of quasi-elastic scattering and fusion are closely related. There are several indications of correlations between nuclear structure effects in fusion and quasi-elastic scattering[144]. These correlations are particularly obvious for quasi-elastic transfer reactions, such as one neutron transfer. It has been found[145,146] that similar to fusion the total one neutron transfer cross sections at energies well above the Coulomb barrier do not depend on the nuclear structure of the reactants but only on the transfer Q-value and neutron binding energies. However, as for fusion, at energies of the order of the Coulomb barrier energy a strong nuclear structure dependence is observed[147].

In addition, it has been found that the isotopic variations of the one neutron transfer cross sections correlate with the variations in sub-barrier fusion enhancement. Among the three possible combinations of ^{58}Ni and ^{64}Ni, for which the sub-barrier fusion enhancement has been discussed in Section 1.4.3, the system ^{58}Ni + ^{64}Ni with the largest sub-barrier fusion enhancement shows also the largest one neutron transfer cross sections[148]. The same correlation is observed[149] for ^{40}Ca + ^{40,44}Ca and for the reactions of ^{16}O and ^{58}Ni with various tin isotopes[150].

The experimental evidence for correlations between fusion and quasi-elastic reactions demands a unified model of nuclear reactions which treats the reflected and the transmitted flux on the same footing. Such a unified model, based on the Hamiltonian 1.1, is now gradually emerging.

1.7 Objectives of this Study

It has been illustrated in the previous sections, that reactions of the nuclear binary system at energies of the order of the Coulomb barrier energy depend sensitively on the internal structure of the system. There is evidence that fusion and quasi-elastic

[143]see e.g. U. Mosel, Treatise on Heavy Ion Science, Vol. 2, Plenum Press, NY (1984) 3.
[144]K.E. Rehm, Proc. of XII Workshop on Nucl. Phys., Argentina, World Scientific (1990) 212.
[145]A.M. van den Berg *et al.*, Phys. Lett. B **194** (1987) 334.
[146]F.L.H. Wolfs *et al.*, Phys. Rev. C **45** (1992) 2283.
[147]W. Reisdorf *et al.*, Z. Phys. A **342** (1992) 411.
[148]J. Wiggins *et al.*, Phys. Rev. C **31** (1985) 1315.
[149]H.A. Aljuwair *et al.*, Phys. Rev. C **30** (1984) 1223.
[150]W. Henning *et al.*, Phys. Rev. Lett. **58** (1987) 318.

scattering are correlated in this dependence.

The internal degrees of freedom of the system couple to the relative motion when the nuclei approach each other. In the eigen-channel model the couplings can be thought to generate a distribution of potential barriers which replace the one-dimensional Coulomb barrier. The understanding of the couplings has been improved recently through the realization that this barrier distribution determines the transmitted flux. A technique has been developed to extract representations of the barrier distribution from precisely measured fusion excitation functions. These representations are direct evidence for the occurrence of channel-coupling in fusion.

Inspired by the quest for a unified approach to the nuclear binary problem, it is an objective of this thesis to extend the technique of extracting barrier distribution representations to experimental data for quasi-elastic scattering, which dominates the reflected flux in nuclear collisions at barrier energies. The aim is to establish experimentally direct evidence of the influence of barrier distributions on quasi-elastic channels, such as elastic and inelastic scattering and transfer reactions. It is intended to achieve this by extracting representations of the barrier distribution from quasi-elastic scattering excitation functions. Such representations should be complementary to that obtainable from fusion data. It is aimed to test the validity of the quasi-elastic scattering representations of the barrier distribution experimentally over a wide range of projectile and target combinations including ^{16}O, ^{32}S and ^{40}Ca as projectile and ^{90,92,96}Zr, ^{144,154}Sm, ^{186}W and ^{208}Pb as target nuclei.

With the inclusion of quasi-elastic scattering the novel technique to extract barrier distribution representations from experimental data should allow the investigation of the nuclear barrier problem in a complete fashion before invoking any theoretical calculations. It is intended to use quasi-elastic scattering and fusion representations of the barrier distribution to explore couplings to the dominant internal degrees of freedom of the nuclear binary system, which are collective excitations and nucleon transfer. Among the collective excitations, double phonon excitations have been discovered to be of particular importance in some system. Since there is some evidence[151] for double phonon states in ^{90,96}Zr, and the barrier distributions of ^{16}O, ^{28}Si + ^{208}Pb appear to be affected[152,153] by such excitations in ^{208}Pb, this work aims to explore these findings further by studying the systems ^{40}Ca + ^{90,96}Zr and ^{32}S + ^{208}Pb.

[151]G. Molnár, *et al.*, Nucl. Phys. A **500**, (1989) 43.

[152]C.R. Morton *et al.*, Phys. Rev. C **52** (1995) 243.

[153]D.J. Hinde *et al.*, Nucl. Phys. A **592** (1995) 271.

It is also planned to investigate the relative importance of collective excitations and of nucleon transfer for the fusion of the nuclear binary system. The effect of one and two neutron transfer on fusion has been demonstrated for some reactions[154,155]. However, in these systems the effect is rather smaller than expected from the strong phenomenological correlations discussed in Section 1.6.2, which are observed between fusion and transfer reactions in other systems. The comparison of the two reactions ^{40}Ca + ^{90,96}Zr should be particularly well suited to isolate the effects of neutron transfer. The projectile ^{40}Ca is a closed shell nucleus, so that its influence on the fusion process may be negligible. Then the fusion dynamics should be dominated by the properties of the two target nuclei. As pointed out in Section 1.3.1, among the even-even zirconium isotopes ^{96}Zr is the one which is most similar to the neutron-magic ^{90}Zr. Both are spherical with similar shell structures. In both cases the lowest quadrupole and octupole states are moderately collective and may be expected to play a similar role in the fusion dynamics. The two reactions differ, however, distinctively in their neutron transfer Q-values. In the heavier system up to 8 neutrons can be transferred with positive Q-values from ^{96}Zr to ^{40}Ca. In contrast, the Q-values for the respective channels in the lighter system are all negative. It has been proposed[156] that the flow of neutrons between the reactants may initiate fusion at large inter-nuclear separations. As has been pointed out in Section 1.5.4, neutron-flow is expected to correspond to a flat barrier distribution with the left hand edge of the distribution being the lowest energy for which the distance of closest approach allows neutrons to transfer between the two potential wells[157]. If neutron-flow occurs, the system ^{40}Ca + ^{96}Zr is an ideal candidate for it and the effect should be reflected in the barrier distribution.

The observation of neutron-flow would establish the missing link between the two main theoretical approaches to the fusion of the nuclear binary system, which are based on the truncation and the macroscopic limit of the generalized barrier problem, respectively. Whereas coupling to strong collective excitations appears to dominate in lighter systems, which can be described in the truncation limit, massive nucleon transfer and dissipation are observed for heavy systems demanding a description within the macroscopic limit. The understanding of the transition between the truncation and the macroscopic limit in the nuclear binary system

[154]C.R. Morton *et al.*, Phys. Rev. Lett. **72** (1994) 4074.

[155]A.M. Stefanini *et al.* Phys. Rev. C **52** (1995) R1727.

[156]P.H. Stelson, Phys. Lett. B **205** (1988) 190.

[157]W. von Oertzen *et al.* Z. Phys. A **326** (1987) 463.

would be beneficial for the further exploitation of this system as a micro-laboratory of the generalized barrier problem.